applied optics

Multifocal diffractive lens design in ophthalmology

Aizhong Zhang

Lightrino, LLC, 304 Building 59, Eastman Business Park, 1669 Lake Ave., Rochester, New York 14652, USA (e-mail: harbin100@gmail.com)

Received 31 July 2020; revised 27 September 2020; accepted 28 September 2020; posted 29 September 2020 (Doc. ID 403554); published 26 October 2020

Multifocal diffractive lenses are used widely in ophthalmology. This paper provides a general mathematical formula to summarize various multifocal diffractive lens designs and introduces a novel, design: the subzonal multifocal diffractive (SMUD) lens. Analytical and numerical methods of SMUD lens design are elaborated in detail. A number of trifocal and quadrifocal SMUD lens designs of high diffraction efficiency are presented. Fresnel zone spacing factors are introduced to take into account the incidence of a converging or diverging beam and the curvature of the substrate on which the diffractive surface is created. Apodization and ophthalmic astigmatism correction related to diffractive lenses are also discussed.

https://doi.org/10.1364/AO.403554

1. INTRODUCTION

Multifocal diffractive lenses are diffractive elements that distribute input optical energy to more than one focal point. This unique multifocal property is a useful alternative to the accommodation of an eye, which is gradually lost with aging [1]. Clinically, the most common multifocal diffractive lenses in ophthalmology are intraocular lenses, which are used widely to replace clouded natural crystalline lenses of cataract patients to restore vision. It is estimated that about 30 million people will have cataract by 2020 in United States alone [2], and worldwide cataract blind people will increase to 40 million in 2025 [3]. Cataract surgery is one of the most common surgical procedures in the world [4], which could significantly improve the quality of life for cataract patients. Multifocal diffractive lenses have also been used in the form of contact lenses, intracorneal lenses, etc. Compared with monofocal intraocular lenses, multifocal intraocular lenses could enable patients to achieve spectacle independence [5]. Further, multifocal lenses can improve vision for people with presbyopia [6].

Over the past several decades, many multifocal diffractive optical designs have been developed [7–10]. Apodization in diffractive efficiencies was introduced to emphasize distant vision in mesopic condition and reduce glares and halos [11]. Even though diffractive lenses with hyperbolic or elliptical outlines to correct ophthalmic astigmatism have been described [12], refractive toric intraocular lenses are more commonly used to correct ophthalmic astigmatism in cataract surgeries [13–15].

This paper proposes a generalized mathematical formalism to summarize multifocal diffractive lens designs. Further, a novel design method of a subzonal multifocal diffractive (SMUD) lens is described. In a SMUD lens, a Fresnel zone is divided into a series of independent subzones, which allows much more design freedom and more flexible energy allocation into different orders. A list of trifocal and quadrifocal designs with customized diffraction efficiency splitting ratios and effective diffraction efficiency near 90% is presented. Apodization and astigmatism correction related to diffractive lenses in ophthalmology are also briefly discussed.

2. MATHEMATICAL FRAMEWORK

I shall start with plane wave illumination for a diffractive surface on a flat substrate, as shown in Fig. 1. r_j is the radius of the edge of the jth zone of the Fresnel full-period zones. λ_0 is the design wavelength, from which the diffractive profile is defined, and d is the first-order focal length of the diffractive lens [16]. n is the refractive index of the diffractive lens material, and n' is the refractive index of the ambient environment. The origin of the coordinate system is chosen to be the point where the lens vertex intersects with the optical axis. Figure 1(a) presents a diffractive surface with a positive power ($d > 0$), and Fig. 1(b) presents a diffractive surface with a negative power ($d < 0$).

Referring to Fig. 1(a), the optical path length (OPL) of the ray passing through the edge of the jth zone and the ray through the origin differ by an integer j multiplied by the design wavelength:

$$n'\left(\sqrt{d^2 + r_j^2} - d\right) = j\lambda_0. \tag{1}$$

When $d \gg \lambda_0$, i.e., when the diffractive lens has a first-order focal length much longer than the design wavelength, Eq. (1) is simplified as

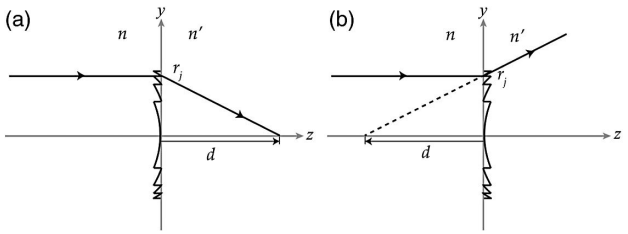

Fig. 1. Fresnel zone boundary determination of a diffractive surface on a flat substrate with plane wave incidence. (a) Diffractive surface with a positive power ($d > 0$) and (b) diffractive surface with a negative power ($d < 0$).

$$r_j^2 = 2j\lambda_0 \frac{d}{n'} = 2j\lambda_0 d', \tag{2}$$

where

$$d' = \frac{d}{n'(\lambda_0)}, \quad d > 0. \tag{3}$$

Referring to Fig. 1(b), the OPL equation at the Fresnel zone boundaries is

$$n'\left(\sqrt{d^2 + r_j^2} + d\right) = j\lambda_0. \tag{4}$$

Similarly, when $|d| \gg \lambda_0$, Eq. (4) is simplified as

$$r_j^2 = -2j\lambda_0 \frac{d}{n'} = 2j\lambda_0 d', \tag{5}$$

where

$$d' = -\frac{d}{n'(\lambda_0)}, \quad d < 0. \tag{6}$$

Apparently, $d' = |d|$ when the ambient environment is air. However, in ophthalmic applications, the ambient environment is usually not air, but aqueous humor, tear film, or other body fluids.

Note that for a diffractive surface with positive power, the OPL is longer for the ray passing through the jth zone edge, compared with the ray passing along the optical axis, while for a diffractive surface with negative power, the OPL is shorter when passing through the jth zone edge.

Using the notation of d', the same formula for r_j^2 is obtained for both positive and negative diffractive surfaces. The diffractive lens Fresnel zone boundaries are found to be periodic in $\rho = r^2$. These boundaries segment the diffractive surface into a central circular zone and surrounding concentric annular zones of equal areas.

To maximize the optical energy at the desired focal point(s), constructive interference from different zones is preferred, and this demands not only the zone boundaries, but also the diffractive lens profile to be periodic in ρ space. The transmission function of the diffractive optical surface can be expressed as

$$\begin{aligned} t(\rho) &= A(\rho)\exp[i\phi(\rho)] \\ &= A(\rho)\exp\{ik(\lambda)[n(\lambda) - n'(\lambda)]\delta(\rho)\}, \end{aligned} \tag{7}$$

where $A(\rho)$ is the electric field absorption, $k = 2\pi/\lambda$ is the wavenumber, and $\delta(\rho)$ is the lens profile thickness. In most ophthalmic lenses, maximum optical throughput is desired, and a transparent diffractive lens with no absorption, i.e., $A(\rho) = 1$, is assumed in the following analysis. Therefore, the transmission function induces different phase delays only at different radial locations.

Since the transmission function $t(\rho)$ is periodic in ρ, it can be expanded into a Fourier series:

$$\begin{aligned} t(\rho) &= \exp[i\phi(\rho)] = \exp\{ik(\lambda)[n(\lambda) - n'(\lambda)]\delta(\rho)\} \\ &= \sum_{m=-\infty}^{+\infty} c_m e^{-i2\pi m\rho/L} = \sum_{m=-\infty}^{+\infty} c_m e^{-\frac{im\pi\rho}{\lambda_0 d'}}, \end{aligned} \tag{8}$$

where $L = 2\lambda_0 d'$ is the period in ρ space, from Eqs. (2) and (5). The Fourier coefficients c_m are given by

$$\begin{aligned} c_m &= \frac{1}{L}\int_0^L t(\rho)e^{i2\pi m\rho/L}\mathrm{d}\rho \\ &= \frac{1}{2\lambda_0 d'}\int_0^{2\lambda_0 d'} \exp\left[ik(n - n')\delta(\rho) + i\frac{m\pi\rho}{\lambda_0 d'}\right]\mathrm{d}\rho. \end{aligned} \tag{9}$$

Apparently, c_m is related directly to the wavelength in use λ (implicitly contained in k), refractive indices of the lens material n and the ambient environment n', and the thickness profile $\delta(\rho)$.

The mth order diffraction efficiency is given by

$$\eta_m = c_m c_m^*. \tag{10}$$

The phase transmission of a thin lens with paraxial approximation is [17]

$$t_{\mathrm{lens}} = \exp\left[-\frac{i\pi n'(\lambda)r^2}{\lambda f}\right] = \exp\left[-\frac{i\pi n'(\lambda)\rho}{\lambda f}\right]. \tag{11}$$

Comparing Eq. (8) with Eq. (11), one can find that the Fourier series represents a series of converging and diverging beams. Each term corresponds to a thin lens with a focal length of

$$f_m = \frac{\lambda_0|d|n'(\lambda)}{\lambda m n'(\lambda_0)}, \tag{12}$$

where $d' = |d|/n'(\lambda_0)$ is used. Evidently, $|d|$ is the first-order ($m = 1$) focal length at the design wavelength λ_0. Further, the optical power is

$$\Phi_m = \frac{1}{f_m} = \frac{\lambda m n'(\lambda_0)}{\lambda_0|d|n'(\lambda)}, \tag{13}$$

i.e., the optical power is directly proportional to wavelength λ at a given order m.

If the ambient environment is air, or if the dispersion of the ambient environment is small and negligible, Eqs. (12) and (13) could be simplified into more common forms of [16]

$$f_m = \frac{\lambda_0|d|}{\lambda m}, \tag{14}$$

$$\Phi_m = \frac{1}{f_m} = \frac{\lambda m}{\lambda_0|d|}. \tag{15}$$

The Fourier series basis functions in Eq. (8) are chosen to have the form of $e^{-i2\pi m\rho/L}$, instead of $e^{i2\pi m\rho/L}$. This is because $e^{-i\omega t}$ time dependence is implicitly assumed, and the common practice is to make the positive mth order correspond to a converging beam with a positive focal length f_m [16].

Equations (2) and (12) demonstrate that the focal point locations are determined by the boundary positions in a diffractive lens. Equations (9) and (10) further show that the diffraction efficiency, i.e., the output energy allocation among all focal points, is determined completely by the lens structure within one period.

The diffractive lens profile $\delta(\rho)$ can be any periodic structure of ρ. The simplest profile is periodically linear in ρ, and hence quadratic in r.

In the following, I propose a generalized form of the phase profile to describe multifocal diffractive lenses that are periodically linear in ρ:

$$\phi(\rho;\lambda) = k(\lambda)[n(\lambda)-n'(\lambda)]\delta_0\left(j-\frac{\rho}{2\lambda_0 d'}\right)$$
$$= 2\pi\alpha\beta\left(j-\frac{\rho}{2\lambda_0 d'}\right)$$
$$\rho_j \le \rho < \rho_{j+1}, \quad \rho_j = 2j\lambda_0 d', \tag{16}$$

where δ_0 is the step height, i.e., the thickness difference at the zone boundaries. α is a parameter first introduced by Dammann [18], which is the wavelength detuning factor to account for the optical path difference for wavelengths other than the design wavelength:

$$\alpha = \frac{\phi(\lambda)}{\phi(\lambda_0)} = \frac{\lambda_0[n(\lambda)-n'(\lambda)]}{\lambda[n(\lambda_0)-n'(\lambda_0)]}. \tag{17}$$

When $\alpha = 1$, $\lambda = \lambda_0$, Eq. (16) is reduced to a monochromatic design.

The parameter β is defined as

$$\beta = [n(\lambda_0)-n'(\lambda_0)]\delta_0/\lambda_0. \tag{18}$$

I shall refer to β as a phase step factor, since $2\pi\beta = k(n-n')\delta_0$ is the phase step immediately across the zone boundaries at the design wavelength λ_0. $\beta > 0$ corresponds to a positive lens, and $\beta < 0$ corresponds to a negative lens.

Note that the wavelength detuning factor α is determined by the wavelength in use and the refractive indices of the lens material and the ambient environment. α is independent of the lens thickness profile. Once an application is determined, α is usually set to a specific number or limited to a narrow range.

In contrast, the phase step factor β is related directly to the lens profile, and β is independent of the wavelength in use. Hence, it is the deliberate choice of β, i.e., the choice of the thickness profile and refractive indices, that characterizes a certain diffractive lens design.

Based on Eqs. (9) and (16),

$$c_m = \frac{1}{2\lambda_0 d'}\int_0^{2\lambda_0 d'} \exp\left[-i\frac{2\pi\alpha\beta\rho}{2\lambda_0 d'} + i\frac{m\pi\rho}{\lambda_0 d'}\right] d\rho$$
$$= e^{i\pi(m-\alpha\beta)}\,\mathrm{sinc}(m-\alpha\beta), \tag{19}$$

where $\mathrm{sinc}(x) = \frac{\sin(\pi x)}{\pi x}$.

From Eq. (10), the diffraction efficiency

$$\eta_m = c_m c_m^* = \mathrm{sinc}^2(m-\alpha\beta). \tag{20}$$

3. CASE ANALYSIS OF MULTIFOCAL DIFFRACTIVE LENSES

A. Monochromatic Analysis

In this section, I shall analyze detailed cases of multifocal diffractive lenses at the design wavelength λ_0 ($\alpha = 1$). Different design forms are explored by manipulating the phase step factor β.

When $\beta = 1$, Eq. (16) is reduced to the classical kinoform design [16,18], which is a monofocal diffractive lens at the design wavelength λ_0 with a focal length of d.

When $\beta = 0.5$, Eq. (16) is reduced to a bifocal lens [19], as shown in Figs. 2(a) and 2(b). At the design wavelength λ_0, the zeroth order and the first order each has a diffraction efficiency of $(2/\pi)^2 \approx 40.53\%$, and the remaining ~19% energy is distributed among higher orders. Similarly, $\beta = -0.5$ corresponds to a negative bifocal lens, with ~40.53% of energy in each main focus, as shown in Figs. 2(c) and 2(d).

When $\beta = p$, where p is an integer, Eq. (16) is reduced to a multiorder diffractive (MOD) lens or a higher-order diffractive

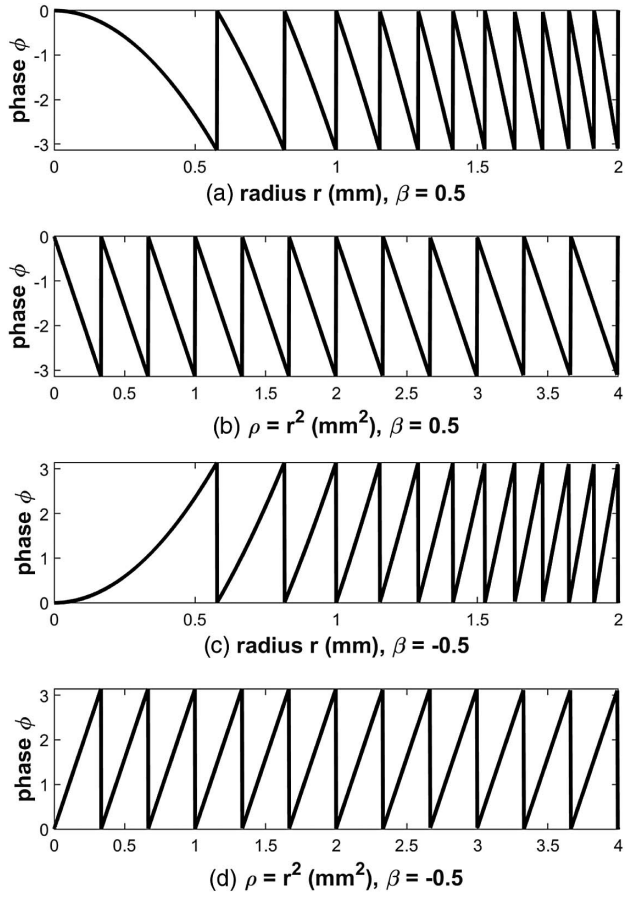

Fig. 2. Phase profiles of two bifocal lenses with respect to radius r and $\rho = r^2$. (a), (b) Positive bifocal lens ($d' = 300$ mm, $\beta = 0.5$); (c), (d) negative bifocal lens ($d' = 300$ mm, $\beta = -0.5$). The phase profiles are periodically linear in ρ. The design wavelength $\lambda_0 = 555$ nm for both lenses.

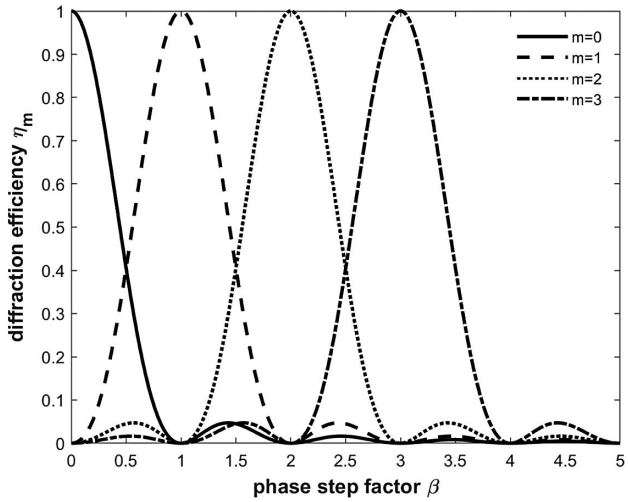

Fig. 3. Diffraction efficiency variation with the phase step factor β for the design wavelength λ_0 ($\alpha = 1$).

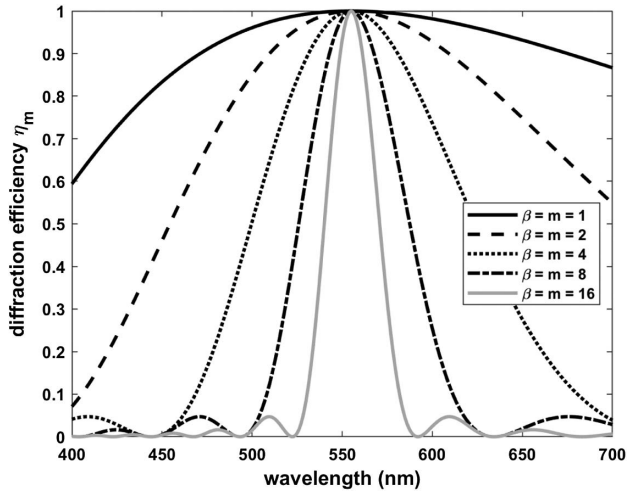

Fig. 4. Diffraction efficiency dependence on wavelength of MOD lenses, assuming no material dispersion ($\alpha \approx \lambda_0/\lambda$). The diffraction peak wavelength bandwidth continuously decreases with increasing order m. The design wavelength $\lambda_0 = 555$ nm.

lens, as described by Faklis and Morris [20]. Let $d = pF_0$, this MOD lens is monofocal with a focal length of F_0 for the design wavelength λ_0. The monofocality of the MOD lens is clearly shown in Fig. 3; when β equals an integer $p = 1, 2, 3$, the corresponding diffraction efficiency of the pth order becomes unity at λ_0. This MOD lens is essentially designed with a first-order focal length of $d = pF_0$, while the integer phase step factor $\beta = p$ ensures 100% diffraction efficiency (under scalar diffraction theory) at the p th-order focal point with a focal length of $d/p = F_0$.

As $|\beta|$ gets larger, the step height at the zone boundary increases, and the shadowing effect will decrease the diffraction efficiency [21]. On the other hand, because of the quadratic dependence on r of the diffractive surface profile, the spacing between adjacent zone boundaries gets very close at the rim of the diffractive lens, which poses a challenge for fabrication. In order to increase the manufacturability of the diffractive lens, MOD lens designs with $\beta = p$ are sometimes used at the periphery part of the lens to increase the zone spacing and step height, with increasing p toward the periphery, while maintaining the same focal length. The periphery region with increasing integer $\beta = p$ is referred to as the "superzone" by Futhey [10].

B. Chromatic Analysis

When the incident light wavelength differs from the design wavelength λ_0, the wavelength detuning factor $\alpha \neq 1$, and the chromatic performance of a diffractive lens has to be taken into account.

Based on Eq. (12), at a given order, there will be defocus at different wavelengths, which is the longitudinal color or axial color. From Eq. (13), the Abbe number at mth order can be calculated at three reference wavelengths: λ_s, λ_i, and λ_l, which represent short, intermediate, and long wavelength, respectively:

$$\nu = \frac{\Phi_m(\lambda_i)}{\Phi_m(\lambda_s) - \Phi_m(\lambda_l)} = \frac{\lambda_i / n'(\lambda_i)}{\lambda_s / n'(\lambda_s) - \lambda_l / n'(\lambda_l)}$$

$$\approx \frac{\lambda_i}{\lambda_s - \lambda_l}. \tag{21}$$

Note that ν is independent of the refractive index of the lens material and the specific order number m. The last step approximation in Eq. (21) assumes that the ambient environment material dispersion is small. In the visible spectrum, if the d, F, C Fraunhofer emission lines of 656.3 nm, 587.6 nm, and 486.1 nm are used, the Abbe number $\nu \approx -3.45$.

If we ignore the small dispersion of both the diffractive lens and ambient materials, the wavelength detuning factor α in Eq. (17) can be approximated as

$$\alpha \approx \frac{\lambda_0}{\lambda}. \tag{22}$$

With Eq. (22), the MOD lens diffraction efficiency dependence on wavelength is plotted for several representative diffraction orders in Fig. 4. Clearly, the wavelength bandwidth of diffraction efficiency curves gets smaller with increasing orders [20].

Generally speaking, in the vicinity of a diffraction peak, the diffraction efficiency will drop from the peak with the deviation from the optimal step height (related directly to β) or the deviation of the wavelength in use λ from the design wavelength λ_0. To quantify the wavelength bandwidth, I propose a definition of diffraction peak wavelength bandwidth as the wavelength width at which the diffraction efficiency drops to $(2/\pi)^2$ of its peak value, since this choice is analogous to a half-width of $\beta = 0.5$, when $\alpha = 1$, as shown in Fig. 3. This definition will simplify the mathematical calculation. With the approximation of Eq. (22), Eq. (20) is reduced to

$$\eta_m \approx \operatorname{sinc}^2\left(m - \frac{\lambda_0}{\lambda}\beta\right). \tag{23}$$

The diffraction peak happens at approximately

$$\beta = (\lambda/\lambda_0)m. \tag{24}$$

Specifically, for a MOD lens, $\beta = p = m$, and the two boundaries of the peak wavelength bandwidth according to

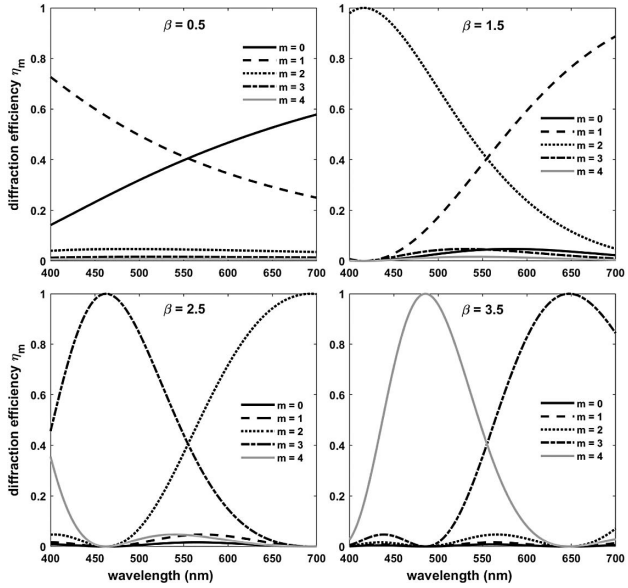

Fig. 5. Bifocal lens diffraction efficiency dependence on wavelength, for $\beta = 0.5, 1.5, 2.5$, and 3.5, assuming no material dispersion ($\alpha \approx \lambda_0/\lambda$). The design wavelength $\lambda_0 = 555$ nm.

the above definition can be found by setting $m - (\lambda_0/\lambda)m = \pm 1/2$; hence, the bandwidth

$$\Delta\lambda = \frac{\lambda_0}{m - \frac{1}{4m}}, \tag{25}$$

which is a monotonically decreasing function with m, for $m > 0$.

Even though Eq. (25) is derived for a MOD lens, the general conclusion that the wavelength bandwidth decreases with increasing diffraction order m still holds, because for a given β, it is always possible to find a wavelength λ_0' at which the lens is a MOD lens based on Eq. (24).

For example, consider a bifocal design with $\beta = 0.5$ at design wavelength $\lambda_0 = 555$ nm. This lens is a monofocal lens at $\lambda_0' = 0.5\lambda_0 = 277.5$ nm, if material dispersion is ignored. A plot similar to Fig. 4 can be generated at a pseudo-design wavelength λ_0' to analyze the peak wavelength bandwidth of the diffraction efficiency in the visible spectrum.

If only the diffraction output at the design wavelength λ_0 is of concern, based on Fig. 3, any $\beta = (2p - 1)/2$, where p is an integer, will generate the same bifocal output, and the only difference is that different diffraction orders are being used. However, Fig. 5 shows the bifocal lens diffraction efficiency dependence on wavelength with four representative phase step factors $\beta = 0.5, 1.5, 2.5$, and 3.5, with Eq. (22) approximation. Clearly, $\beta = 0.5$ has the widest wavelength bandwidth for the two desired orders.

It is because of the relatively large wavelength bandwidth that usually lower orders are used for broadband diffractive lens designs. For a monofocal lens, the first order is usually used. For a bifocal lens, the zeroth order and the first order are usually used. For a trifocal design, the zeroth, first, and second orders are usually used. A similar trend holds for multifocal diffractive lenses with more foci.

4. SUBZONAL MULTIFOCAL DIFFRACTIVE LENS

Even though the generalized form Eq. (16) is able to summarize many different types of multifocal diffractive lenses, it unnecessarily requires a constant phase step factor β within each zone. I propose a novel design (patent pending [22]) of a multifocal diffractive lens with segmented subzones within each Fresnel zone, and each subzone has a phase profile independent of other subzones within the same Fresnel zone. The subzones are not necessarily of equal areas. The whole structure still remains periodic in ρ to optimize the diffraction efficiency. I shall refer to this novel type of lens as a SMUD lens.

The main advantage of a SMUD lens is that it gives lens designers much more freedom in phase profile configuration and thus enables more flexible energy allocation among different diffraction orders. With careful segmentation of each zone, and proper choice of the diffractive profile of each subzone, multifocal diffractive lenses with desired energy distribution at three or even more foci can be achieved.

A. Two-Subzone SMUD Lens

I shall start with a two-subzone SMUD lens, which has the following phase profile [22]:

$$\phi(\rho; \lambda) = 2\pi\alpha\beta_s\left(j - \frac{\rho}{2\lambda_0 d'}\right), \tag{26}$$

where

$$\beta_s = \begin{cases} \beta_1, & j \le \frac{\rho}{2\lambda_0 d'} < j + \gamma \\ \beta_2, & j + \gamma \le \frac{\rho}{2\lambda_0 d'} < j + 1. \end{cases} \tag{27}$$

γ is a ratio of the first type subzone area over a full Fresnel zone area. $\gamma \in [0, 1]$, and when $\gamma = 0$ or 1, the two-subzone SMUD lens is reduced to a diffractive lens with a constant phase step factor. This two-subzone SMUD lens is periodically linear in ρ. Because of this periodicity, the transmission $t(\rho)$ can still be expanded as a Fourier series, and based on Eq. (9), the coefficient

$$\begin{aligned} c_m &= \frac{1}{2\lambda_0 d'}\left\{\int_0^{2\gamma\lambda_0 d'} \exp\left[-i\frac{2\pi\alpha\beta_1\rho}{2\lambda_0 d'} + i\frac{m\pi\rho}{\lambda_0 d'}\right] d\rho \right. \\ &\quad \left. + \int_{2\gamma\lambda_0 d'}^{2\lambda_0 d'} \exp\left[-i\frac{2\pi\alpha\beta_2\rho}{2\lambda_0 d'} + i\frac{m\pi\rho}{\lambda_0 d'}\right] d\rho\right\} \\ &= \gamma e^{i\pi\gamma(m-\alpha\beta_1)}\mathrm{sinc}[\gamma(m - \alpha\beta_1)] + (1 - \gamma) \\ &\quad \times e^{i\pi(1+\gamma)(m-\alpha\beta_2)}\mathrm{sinc}[(1 - \gamma)(m - \alpha\beta_2)]. \end{aligned} \tag{28}$$

From Eq. (10), the m th-order diffraction efficiency

$$\begin{aligned} \eta_m &= \gamma^2\mathrm{sinc}^2[\gamma(m - \alpha\beta_1)] + (1 - \gamma)^2\mathrm{sinc}^2[(1 - \gamma)(m - \alpha\beta_2)] \\ &\quad + 2\gamma(1 - \gamma)\mathrm{sinc}[\gamma(m - \alpha\beta_1)]\mathrm{sinc}[(1 - \gamma)(m - \alpha\beta_2)] \\ &\quad \times \cos\{\pi[\gamma(m - \alpha\beta_1) - (1 + \gamma)(m - \alpha\beta_2)]\}. \end{aligned} \tag{29}$$

It is important to point out that c_m and η_m are independent of the choice of the first-order focal length d and $d' = |d|/n'$. Further, the sinc cross term of different subzones in Eq. (29) is a significant part of the total diffraction efficiency, which can contribute up to 50% of the total diffraction efficiency, and the sinc cross term can be negative.

The additional degrees of freedom of a different phase step factor and an arbitrary subzonal division ratio γ make a two-subzone SMUD lens especially useful for trifocal diffractive lens design, as illustrated below.

When $\gamma = 0.5$, all the subzones in a two-subzone SMUD lens are of equal areas. This special case is equivalent to some multifocal diffractive lenses in the literature [8,9,23]. If the subzone numbers (instead of the entire Fresnel zone numbers) are counted, $\gamma = 0.5$ corresponds to a design with alternating odd and even numbered zones of equal areas, where all the odd numbered zones share one phase profile in ρ, and all the even numbered zones share a different phase profile in ρ.

The diffraction efficiency of the two-subzone SMUD lens with $\gamma = 0.5$ is

$$\eta_m = \frac{1}{4}\mathrm{sinc}^2\left[\frac{1}{2}(m-\alpha\beta_1)\right] + \frac{1}{4}\mathrm{sinc}^2\left[\frac{1}{2}(m-\alpha\beta_2)\right] + \frac{1}{2}\mathrm{sinc}\left[\frac{1}{2}(m-\alpha\beta_1)\right]\mathrm{sinc}\left[\frac{1}{2}(m-\alpha\beta_2)\right] \times \cos\left\{\pi\left[\frac{1}{2}(m-\alpha\beta_1) - \frac{3}{2}(m-\alpha\beta_2)\right]\right\}. \tag{30}$$

Further, when $\beta_1 = \beta_2 = \beta$, simple calculation demonstrates that Eq. (30) is reduced to Eq. (20).

Figure 6 is created with Eq. (29). It presents the diffraction efficiency dependence on different β_1 and β_2 pairs of the first three diffraction orders of three two-subzone SMUD lenses with three representative $\gamma = 0.25, 0.5, 0.75$ at the design wavelength λ_0.

The diagonal line of $\beta_1 = \beta_2$ in Fig. 6 presents a lens with a constant phase step factor, which has already been analyzed in Fig. 3. Similar to Fig. 3, the diffraction efficiency pattern jumps at integer $\beta = m$ along the diagonal line while maintaining exactly the same form.

Figure 7 presents a zoomed-out diffraction efficiency plot of the same two-subzone SMUD lenses as in Fig. 6, but both β_1 and β_2 are in a larger range of 20 to 20. A cross pattern is consistent throughout all the subplots. The cross center is located at $\beta_1 = \beta_2 = m$, and the two orthogonal lines that form the cross are $\beta_1 = m$ and $\beta_2 = m$, respectively. At these two lines, at least one subzone is "blazed," i.e., of the right profile for maximum diffraction efficiency at the mth order.

When $\beta_1 = m$, and $\alpha = 1$, the diffraction efficiency

$$\eta_m = \gamma^2 + (1-\gamma)^2\mathrm{sinc}^2[(1-\gamma)(m-\beta_2)] + 2\gamma(1-\gamma) \times \mathrm{sinc}[(1-\gamma)(m-\beta_2)]\cos[-\pi(1+\gamma)(m-\beta_2)]. \tag{31}$$

When $\beta_2 \to \infty$, all sinc terms $\to 0$; hence, $\eta_m \to \gamma^2$. The specific case of $\gamma = 0.5$ is plotted in Fig. 8. It is noticeable that

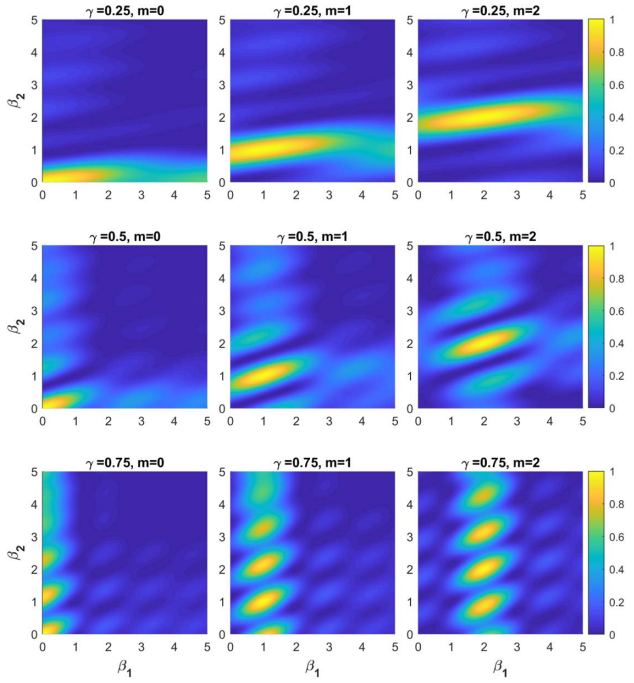

Fig. 6. Diffraction efficiency variation with the phase step factors β_1 and β_2, both in the range of 0-5, for a two-subzone SMUD lens at the design wavelength λ_0 ($\alpha = 1$).

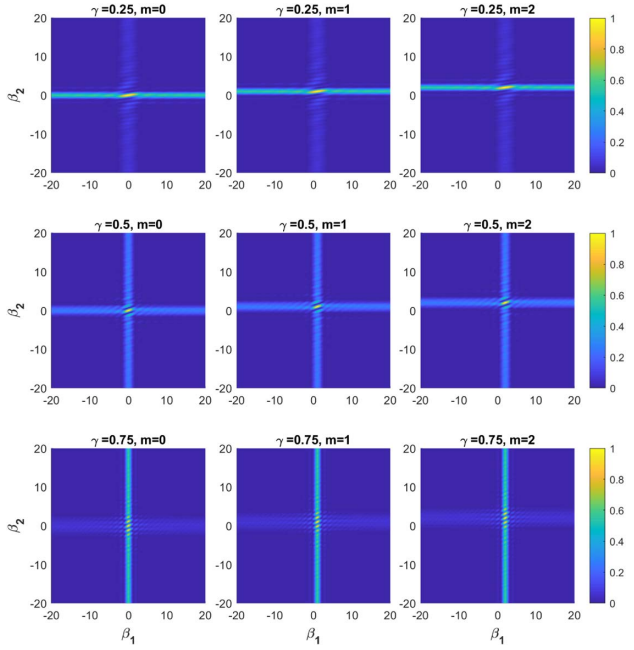

Fig. 7. Diffraction efficiency variation with the phase step factors β_1 and β_2, both in a larger range of 20 to 20, for the design wavelength λ_0 ($\alpha = 1$).

the diffraction efficiencies at different orders sum up to larger than one for some β_2 in Fig. 8. The reason is that Fig. 8 is not the diffraction efficiencies for multiple diffraction orders of the same structure. In a SMUD lens, the profile of each subzone is completely independent of other subzones within the

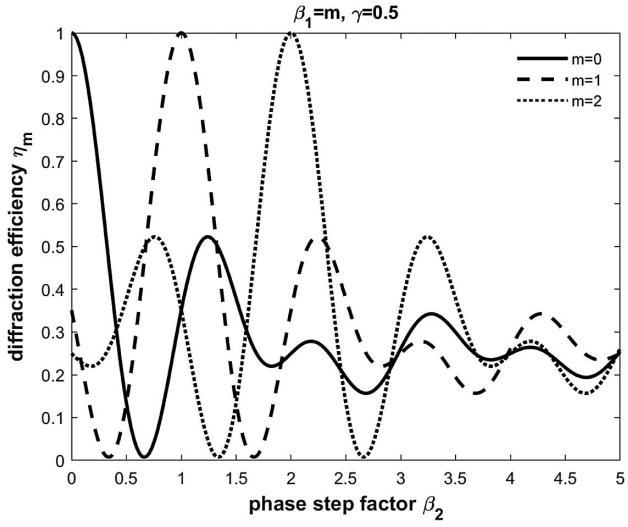

Fig. 8. Diffraction efficiency variation with the phase step factors β_2 for the special case of $\beta_1 = m$, $\gamma = 0.5$ at the design wavelength λ_0 ($\alpha = 1$).

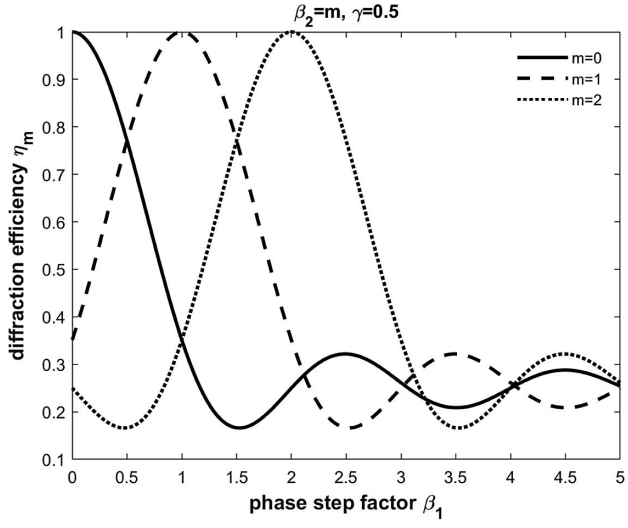

Fig. 9. Diffraction efficiency variation with the phase step factors β_1 for the special case of $\beta_2 = m$, $\gamma = 0.5$ at the design wavelength λ_0 ($\alpha = 1$).

same Fresnel zone. Hence, β_1 and β_2 are not related. $\beta_1 = m$ is assumed in Fig. 8, so the SMUD lens profile changes with the diffraction order m, and the sum of η_m of multiple diffraction orders of different lenses can be larger than one.

When $\beta_2 = m$, and $\alpha = 1$, the diffraction efficiency

$$\eta_m = (1-\gamma)^2 + \gamma^2 \mathrm{sinc}^2[\gamma(m-\beta_1)] + 2\gamma(1-\gamma)\mathrm{sinc}[\gamma(m-\beta_1)]\cos[\pi\gamma(m-\beta_1)]. \quad (32)$$

Similarly, when $\beta_1 \to \infty$, all sinc terms $\to 0$; hence, $\eta_m \to (1-\gamma)^2$. The specific case of $\gamma = 0.5$ is plotted in Fig. 9.

The above analysis can be used to explain the cross feature in Fig. 7. For example, at $\gamma = 0.25$, the bright horizontal line of the cross at large β_1 corresponds to $\eta_m \to (1-0.25)^2 = 0.5625$, while the relatively dimmer vertical line of the cross at large β_2 corresponds to $\eta_m \to 0.25^2 = 0.0625$. At $\gamma = 0.75$, the diffraction efficiency of these two lines of the cross are of opposite values. At $\gamma = 0.5$, both lines of the cross correspond to $\eta_m \to 0.5^2 = 0.25$.

For a trifocal design of a two-subzone SMUD lens, I shall focus on the zeroth, first, and second diffraction orders for the phase step in the range of β_1, $\beta_2 \in [0, 2]$ in order to have good diffraction efficiencies in the entire visible spectrum, for reasons discussed in the chromatic analysis in Section 3.

Depending on the desired diffraction efficiency allocation among different orders, different merit functions can be used to find a good trifocal design solution space. For example, if equal energy splitting is desired for the three foci in a trifocal design, a parameter of the sum of squares (SS) can be used:

$$\mathrm{SS} = (\eta_0 - \eta_1)^2 + (\eta_0 - \eta_2)^2 + (\eta_1 - \eta_2)^2. \quad (33)$$

By minimizing SS, we can find designs of β_1, β_2 that correspond to substantially equal diffraction energy output.

More generally, the SS can be defined as

$$\mathrm{SS} = \left(\frac{\eta_0}{w_0} - \frac{\eta_1}{w_1}\right)^2 + \left(\frac{\eta_0}{w_0} - \frac{\eta_2}{w_2}\right)^2 + \left(\frac{\eta_1}{w_1} - \frac{\eta_2}{w_2}\right)^2, \quad (34)$$

where w_0, w_1, and w_2 are the weighting factors, and $w_0 : w_1 : w_2$ represents the desired diffraction efficiency splitting ratio of the first three orders.

Meanwhile, in a trifocal design employing the first three orders, light diffracted into higher orders is not used and serves as a background that will lower the image contrast. The effective diffraction efficiency of the first three orders is

$$\eta_{\mathrm{eff}} = \eta_0 + \eta_1 + \eta_2. \quad (35)$$

A good design will have the desired diffraction efficiency splitting ratio, i.e., a minimized SS, while maximizing the effective diffraction efficiency η_{eff}, and there is often a trade-off between these two goals.

As a numerical analysis example, I search for trifocal designs with equal energy splitting, i.e., the weighting factor target of $w_0 : w_1 : w_2 = 1 : 1 : 1$. The search is done for the design wavelength λ_0 ($\alpha = 1$), with γ in the range of 0-1 with an increment of 0.01, and both β_1 and β_2 in the range of 0-2 with an increment of 0.01, for chromatic control. If the conditions of $\mathrm{SS} < 0.001$ and $\eta_{\mathrm{eff}} > 80\%$ are required, a total of 362 trifocal design solutions can be found with γ in the range of [0.42, 0.62], the maximum $\eta_{\mathrm{eff,max}} = 84.71\%$, and the minimum $\mathrm{SS}_{\mathrm{min}} = 2.3 \times 10^{-6}$.

Table 1 lists several representative trifocal design solutions that meet the above requirements. Designs #1 and #2 are for $\gamma = 0.5$, which means the subzones are of equal areas, and they form an antisymmetric pair. Designs #3 and #4 generate the largest effective diffraction efficiency η_{eff} of about 85%. The profile of designs #3 and #4 are presented in Figs. 10 and 11. Designs #5 and #6 give the smallest SS, which means the energy is most evenly distributed in the three orders. Within the current design space, effective diffraction efficiency larger

Table 1. Representative Trifocal Design Solutions for a Two-Subzone SMUD Lens with An Equal Splitting Ratio of $w_0 : w_1 : w_2 = 1 : 1 : 1$ as the Target ($\alpha = 1$)

#	γ	β_1	β_2	η_0	η_1	η_2	η_{eff}	SS
1	0.50	0.68	1.31	28.18%	28.43%	27.68%	84.29%	8.7×10^{-5}
2	0.50	1.32	0.69	27.68%	28.43%	28.18%	84.29%	8.7×10^{-5}
3	0.51	0.73	1.32	27.21%	29.32%	28.19%	84.71%	6.7×10^{-4}
4	0.51	1.27	0.68	28.19%	29.32%	27.21%	84.71%	6.7×10^{-4}
5	0.44	0.47	1.28	27.10%	27.09%	27.20%	81.39%	2.3×10^{-6}
6	0.44	1.53	0.72	27.20%	27.09%	27.10%	81.39%	2.3×10^{-6}

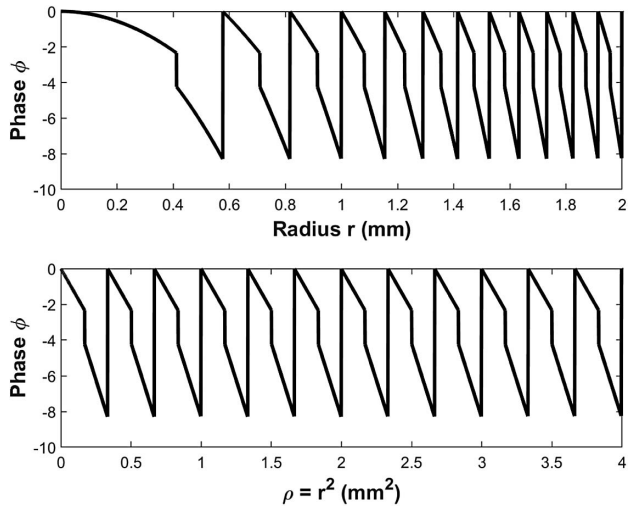

Fig. 10. Phase profile of a trifocal lens (design #3) with respect to radius r (above) and ρ (below). The phase profile is periodically linear in ρ. The specific design parameters of this profile are: $\lambda_0 = 555$ nm, $d' = 300$ mm, $\alpha = 1$, $\beta_1 = 0.73$, $\beta_2 = 1.32$, $\gamma = 0.51$.

than 85% is achievable; however, the energy will not be as evenly distributed, i.e., those designs will have an SS larger than 0.001.

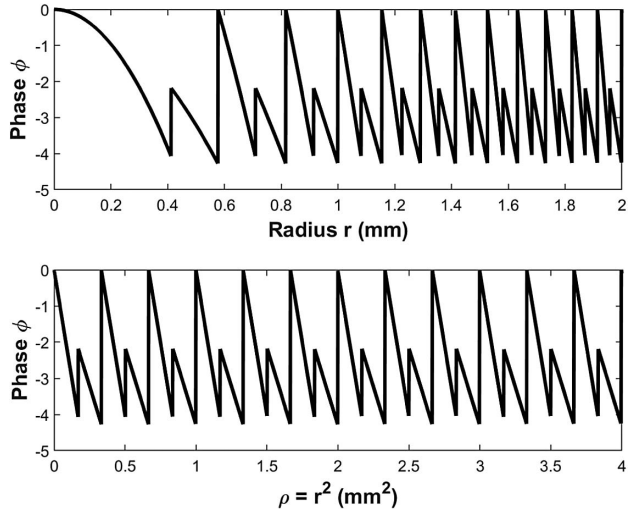

Fig. 11. Phase profile of a trifocal lens (design #4) with respect to radius r (above) and ρ (below). The phase profile is periodically linear in ρ. The specific design parameters of this profile are: $\lambda_0 = 555$ nm, $d' = 300$ mm, $\alpha = 1$, $\beta_1 = 1.27$, $\beta_2 = 0.68$, $\gamma = 0.51$.

Table 2. Representative Trifocal Design Solutions for a Two-Subzone SMUD Lens with a Splitting Ratio of $w_0 : w_1 : w_2 = 2 : 1 : 1$ as the Target to Emphasize the Zeroth Order ($\alpha = 1$)

#	γ	β_1	β_2	η_0	η_1	η_2	η_{eff}	SS
7	0.50	1.08	0.57	41.54%	20.95%	21.35%	83.83%	5.3×10^{-5}
8	0.50	1.04	0.56	42.85%	21.54%	19.89%	84.28%	5.1×10^{-4}
9	0.49	1.05	0.56	43.33%	21.33%	19.63%	84.30%	7.2×10^{-4}
10	0.43	1.27	0.60	40.80%	20.50%	20.50%	81.81%	1.9×10^{-6}
11	0.56	0.56	1.28	40.95%	20.37%	20.45%	81.77%	2.0×10^{-6}

With this trade-off, the final choice of a good multifocal design is application determined.

For intraocular lenses, distant vision, which usually corresponds to the zeroth-order diffraction, is sometimes emphasized. As another numerical analysis example, the same search range and requirements (SS < 0.001, $\eta_{\text{eff}} > 80\%$) as before are used except with a different set of weighting factors of $w_0 : w_1 : w_2 = 2 : 1 : 1$. A total of 474 trifocal design solutions are found with γ in the range of [0.40, 0.61], the maximum $\eta_{\text{eff,max}} = 84.30\%$, and the minimum $\text{SS}_{\text{min}} = 1.9 \times 10^{-6}$.

Table 2 lists several representative trifocal design solutions to emphasize the zeroth-order diffraction. Designs #7 and #8 are for $\gamma = 0.5$ of equal-area subzones. Designs #8 and #9 generate the two largest effective diffraction efficiencies $\eta_{\text{eff}} > 84\%$. Designs #10 and #11 give the two smallest SS, which means the zeroth-order energy is almost twice that of the other two orders.

B. General Linear SMUD Lens Design

The SMUD lenses I have analyzed so far are of two subzones, which are suitable for trifocal designs. SMUD lenses with more subzones of linear ρ dependence can be mathematically described by Eq. (26) and a generalized β_s of G subzones [22]:

$$\beta_s = \begin{cases} \beta_1, & j \le \frac{\rho}{2\lambda_0 d'} < j + \gamma_1 \\ \beta_2, & j + \gamma_1 \le \frac{\rho}{2\lambda_0 d'} < j + \gamma_2 \\ \cdots \\ \beta_g, & j + \gamma_{g-1} \le \frac{\rho}{2\lambda_0 d'} < j + \gamma_g \\ \cdots \\ \beta_G, & j + \gamma_{G-1} \le \frac{\rho}{2\lambda_0 d'} < j + \gamma_G = j + 1 \end{cases}, \tag{36}$$

where $\gamma_1 < \gamma_2 < \gamma_g < \gamma_G = 1$.

From Eqs. (9), (26), and (36), it can be calculated that the generalized Fourier coefficient is

$$\begin{aligned} c_m = {} & \gamma_1 e^{i\pi\gamma_1(m-\alpha\beta_1)} \text{sinc}[\gamma_1(m-\alpha\beta_1)] \\ & + (\gamma_2 - \gamma_1) e^{i\pi(\gamma_2+\gamma_1)(m-\alpha\beta_2)} \text{sinc}[(\gamma_2-\gamma_1)(m-\alpha\beta_2)] \\ & + \cdots \\ & + (\gamma_g - \gamma_{g-1}) e^{i\pi(\gamma_g+\gamma_{g-1})(m-\alpha\beta_g)} \text{sinc}[(\gamma_g-\gamma_{g-1})(m-\alpha\beta_g)] \\ & + \cdots \\ & + (1 - \gamma_{G-1}) e^{i\pi(1+\gamma_{G-1})(m-\alpha\beta_G)} \text{sinc}[(1-\gamma_{G-1})(m-\alpha\beta_G)]. \end{aligned} \tag{37}$$

Table 3. Representative Quadrifocal Design Solutions for a Three-Subzone (Including Two-Subzone) SMUD Lens with An Equal Splitting Ratio of $w_0 : w_1 : w_2 : w_3 = 1 : 1 : 1 : 1$ ($\alpha = 1$)

#	γ_1	γ_2	β_1	β_2	β_3	η_0	η_1	η_2	η_3	η_{eff}	SS
12	0	0.5	–	0.5	2.5	21.1%	22.5%	22.5%	21.1%	87.2%	0.00083
13	0	0.5	–	2.5	0.5	21.1%	22.5%	22.5%	21.1%	87.2%	0.00083
14	0	0.6	–	2.3	0.4	23.1%	23.4%	21.6%	18.5%	86.5%	0.0060
15	0	0.6	–	0.7	2.6	18.5%	21.6%	23.4%	23.1%	86.5%	0.0060
16	0.4	0.7	2.1	0.9	0.8	23.9%	23.6%	22.1%	18.8%	88.5%	0.0066
17	0.4	0.7	0.9	2.1	2.2	18.8%	22.1%	23.6%	23.9%	88.5%	0.0066
18	0.4	0.8	2.2	0.9	0.8	21.8%	22.7%	21.5%	21.5%	87.5%	0.00040
19	0.4	0.8	0.8	2.1	2.2	21.5%	21.5%	22.7%	21.8%	87.5%	0.00040

Based on Eqs. (10) and (37), diffraction efficiencies η_m and other related design parameters can be evaluated for these generalized SMUD lenses with more foci.

When $G = 2$, the general design is reduced to a two-subzone SMUD lens, and Eq. (37) reduces to Eq. (28).

When $G = 3$, the general design is reduced to a three-subzone SMUD lens, which is suitable to be used as a quadrifocal lens, and Eq. (37) reduces to

$$\begin{aligned} c_m = {} & \gamma_1 e^{i\pi\gamma_1(m-\alpha\beta_1)}\text{sinc}[\gamma_1(m-\alpha\beta_1)] \\ & + (\gamma_2-\gamma_1)e^{i\pi(\gamma_2+\gamma_1)(m-\alpha\beta_2)}\text{sinc}[(\gamma_2-\gamma_1)(m-\alpha\beta_2)] \\ & + (1-\gamma_2)e^{i\pi(1+\gamma_2)(m-\alpha\beta_3)}\text{sinc}[(1-\gamma_2)(m-\alpha\beta_3)]. \end{aligned} \tag{38}$$

Based on Eqs. (10) and (38), the m th-order diffraction efficiency of a three-subzone SMUD lens is

$$\begin{aligned} \eta_m = {} & \gamma_1^2\text{sinc}^2[\gamma_1(m-\alpha\beta_1)] \\ & + (\gamma_2-\gamma_1)^2\text{sinc}^2[(\gamma_2-\gamma_1)(m-\alpha\beta_2)] \\ & + (1-\gamma_2)^2\text{sinc}^2[(1-\gamma_2)(m-\alpha\beta_3)] \\ & + 2\gamma_1(\gamma_2-\gamma_1)\text{sinc}[\gamma_1(m-\alpha\beta_1)]\text{sinc}[(\gamma_2-\gamma_1)(m-\alpha\beta_2)] \\ & \times\cos\{\pi[\gamma_1(m-\alpha\beta_1)-(\gamma_2+\gamma_1)(m-\alpha\beta_2)]\} \\ & + 2\gamma_1(1-\gamma_2)\text{sinc}[\gamma_1(m-\alpha\beta_1)]\text{sinc}[(1-\gamma_2)(m-\alpha\beta_3)] \\ & \times\cos\{\pi[\gamma_1(m-\alpha\beta_1)-(1+\gamma_2)(m-\alpha\beta_3)]\} \\ & + 2(\gamma_2-\gamma_1)(1-\gamma_2)\text{sinc}[(\gamma_2-\gamma_1)(m-\alpha\beta_2)] \\ & \times\text{sinc}[(1-\gamma_2)(m-\alpha\beta_3)] \\ & \times\cos\{\pi[(\gamma_2+\gamma_1)(m-\alpha\beta_2)-(1+\gamma_2)(m-\alpha\beta_3)]\}. \end{aligned} \tag{39}$$

Apparently, the fact that c_m and η_m are independent of the choice of the first-order focal length d still holds for SMUD lenses with more subzones. Based on Eq. (39), three-subzone SMUD lens design solutions for quadrifocal diffractive lenses can be analyzed. For a quadrifocal lens, the SS can be defined as

$$\begin{aligned} \text{SS} = {} & \left(\frac{\eta_0}{w_0}-\frac{\eta_1}{w_1}\right)^2+\left(\frac{\eta_0}{w_0}-\frac{\eta_2}{w_2}\right)^2+\left(\frac{\eta_0}{w_0}-\frac{\eta_3}{w_3}\right)^2 \\ & +\left(\frac{\eta_1}{w_1}-\frac{\eta_2}{w_2}\right)^2+\left(\frac{\eta_1}{w_1}-\frac{\eta_3}{w_3}\right)^2+\left(\frac{\eta_2}{w_2}-\frac{\eta_3}{w_3}\right)^2, \end{aligned} \tag{40}$$

where w_0, w_1, w_2, and w_3 are the weighting factors of the first four orders.

The effective diffraction efficiency of the first four orders is

$$\eta_{\text{eff}} = \eta_0+\eta_1+\eta_2+\eta_3. \tag{41}$$

As another example, quadrifocal designs with equal energy splitting, i.e., the weighting factor target of $w_0 : w_1 : w_2 : w_3 = 1 : 1 : 1 : 1$, are numerically analyzed. The analysis is done for the design wavelength λ_0 ($\alpha = 1$), with γ_1 and γ_2 in the range of 0-1 with an increment of 0.1, and $\gamma_1 < \gamma_2$. β_1, β_2, and β_3 are all in the range of 0-3 with an increment of 0.1. If the conditions of SS < 0.01 and $\eta_{\text{eff}} > 80\%$ are required, the maximum $\eta_{\text{eff,max}} = 88.5\%$, and the minimum $\text{SS}_{\text{min}} = 4.0 \times 10^{-4}$ are found.

Table 3 lists several representative quadrifocal design solutions that meet the above requirements. Designs #12 – #15 all have $\gamma_1 = 0$, which means the three-subzone SMUD lens is reduced to a two-subzone SMUD lens. When $\gamma_1 = 0$, β_1 does not correspond to any structural parameter, so it can be any number and will not affect the physical lens profile. Designs #16 and #17 have the largest $\eta_{\text{eff,max}} = 88.5\%$, while designs #18 and #19 have the smallest $\text{SS}_{\text{min}} = 4.0 \times 10^{-4}$ within the search range.

One surprising result is that some of the best performing quadrifocal lenses are two-subzone SMUD lenses, instead of three-subzone SMUD lenses. Two-subzone SMUD lenses are potentially easier to manufacture for some fabrication methods, especially for regions near the edge of a diffractive lens, where the spacing between adjacent zones becomes increasingly smaller. Furthermore, quadrifocal lenses with other weighting factor targets could be analyzed following a similar procedure.

SMUD lenses with five or more orders can be analyzed in a similar fashion. However, there is a trade-off between the number of foci of a diffractive lens in use (i.e., the number of object planes in focus) and the image contrast. Generally speaking, the more orders and foci a diffractive lens has, the less light is concentrated into any single order. The light of all other orders serves as background noise that will reduce the image contrast,

and chromatic aberrations generally are more difficult to manage at higher orders. The fine balance is application dependent, and the final choice of an optimal design may be subject to end user preference.

5. GENERALIZED NONLINEAR PROFILES

The diffractive lenses analyzed so far have been chosen to have a diffractive surface profile periodically linear in ρ, due to simplicity. However, a more generalized diffractive lens profile can be expressed as

$$\phi(\rho;\lambda) = -2\pi\alpha\beta_s\left(\frac{\rho}{2\lambda_0 d'} - j\right)^{\epsilon_s}, \tag{42}$$

where ϵ_s is an exponent for the corresponding subzone. For example, $\epsilon_s = 1$ corresponds to a profile that is linear in ρ and quadratic in r. $\epsilon_s = 1.5$ corresponds to a profile that is cubic in r. $\epsilon_s = 2$ corresponds to a profile that is quadratic in ρ and quartic in r. The negative sign in Eq. (42) ensures that a positive β corresponds to a positive power.

An even more generalized form of a SMUD surface profile could be expressed as

$$\phi(\rho;\lambda) = -2\pi\alpha\beta_s\sum_{k=0}^{\infty} a_{sk}\left(\frac{\rho}{2\lambda_0 d'} - j\right)^{k}, \tag{43}$$

where a_{sk} is the coefficient of the kth power of the s th subzone. The phase profile of each subzone is expressed as a power series of $(\rho/2\lambda_0 d' - j)$.

Figure 12 presents two exemplary lenses with nonlinear profiles in ρ. These two profiles are not optimized for diffraction efficiencies; instead, they are intended to present possible profiles of generalized SMUD lenses. Figures 12(a) and 12(b) are of a two-subzone SMUD lens that can be described by Eq. (42), where $\gamma = 0.45$, $\epsilon_1 = 3$, a profile cubic in ρ and hexic in r for the first type subzone; and $\epsilon_2 = 2$, a profile quadratic in ρ and quartic in r for the second type subzone.

Figures 12(c) and 12(d) are of a two-subzone SMUD lens that can be described by Eq. (43). Here, $\gamma = 0.51$. The first type subzone has the form of

$$\phi(\rho) = -2.54\pi\left[0.5\left(\frac{\rho}{2\lambda_0 d'} - j\right) + 1.5\left(\frac{\rho}{2\lambda_0 d'} - j\right)^2 + 0.35\left(\frac{\rho}{2\lambda_0 d'} - j\right)^3\right], \tag{44}$$

and the second type subzone has the form of

$$\phi(\rho) = -1.36\pi\left[0.2\left(\frac{\rho}{2\lambda_0 d'} - j\right) + 0.5\left(\frac{\rho}{2\lambda_0 d'} - j\right)^2 + 1.2\left(\frac{\rho}{2\lambda_0 d'} - j\right)^3 + 0.4\left(\frac{\rho}{2\lambda_0 d'} - j\right)^4\right]. \tag{45}$$

The diffraction efficiencies of these lenses with nonlinear profiles in ρ can be analyzed to select high diffraction efficiency designs in a procedure similar to the previous analyses. Further optimization of a SMUD lens profile can be done with the aid of an optical design software to minimize optical aberration while maximizing diffraction efficiencies.

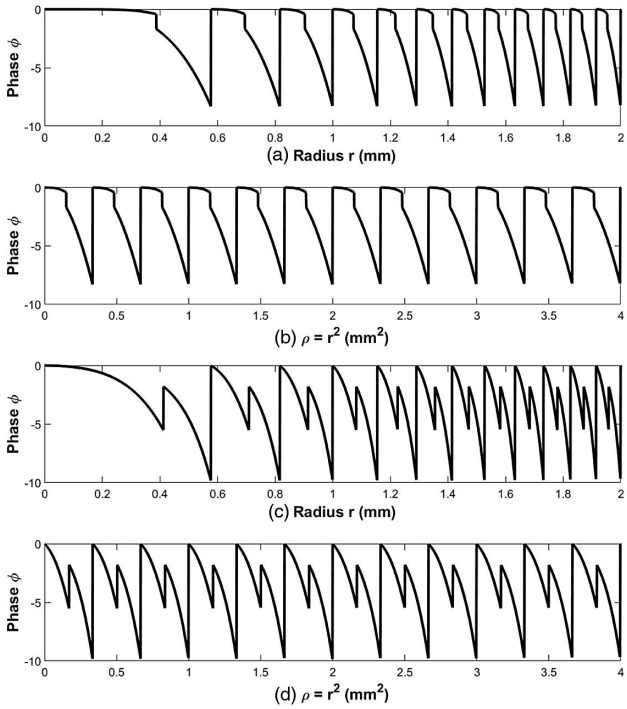

Fig. 12. Generalized phase profiles of two diffractive lenses with respect to radius r and $\rho = r^2$. The profiles are nonlinear in ρ. (a), (b) Two-subzone SMUD lens, $\epsilon_1 = 3$ and $\epsilon_2 = 2$; (c), (d) two-subzone SMUD lens with a phase profile described by Eqs. (44) and (45).

6. CONVERGING AND DIVERGING BEAM INCIDENCE

The above analyses are for plane wave incidence with the diffractive surface on a flat substrate. However, sometimes, the diffractive surfaces should be optimized for converging or diverging beam incidence. For example, in the case of an intraocular lens, because the cornea has a positive power of about 43 diopters, the incident light on the intraocular lens is already a converging beam.

Figure 13 presents six different cases of a diffractive surface of a positive or negative power on a flat substrate with a converging or diverging incident beam. t is the distance from the origin to the center of the incident beam. $t > 0$ corresponds to a converging beam, and $t < 0$ corresponds to a diverging beam.

Referring to Fig. 13(a), the OPL passing the Fresnel zone boundaries in this setup satisfies

$$-nt + n'd + j\lambda_0 = n'\sqrt{d^2 + r_j^2} - n\sqrt{t^2 + r_j^2}. \tag{46}$$

Square both sides of Eq. (46), and it can be rearranged as

$$(n^2 r_j^2 + n'^2 r_j^2 + 2nn'td + 2ntj\lambda_0 - 2n'dj\lambda_0 - j^2\lambda_0^2)^2 = 4n^2 n'^2[t^2 d^2 + r_j^2(t^2 + d^2) + r_j^4]. \tag{47}$$

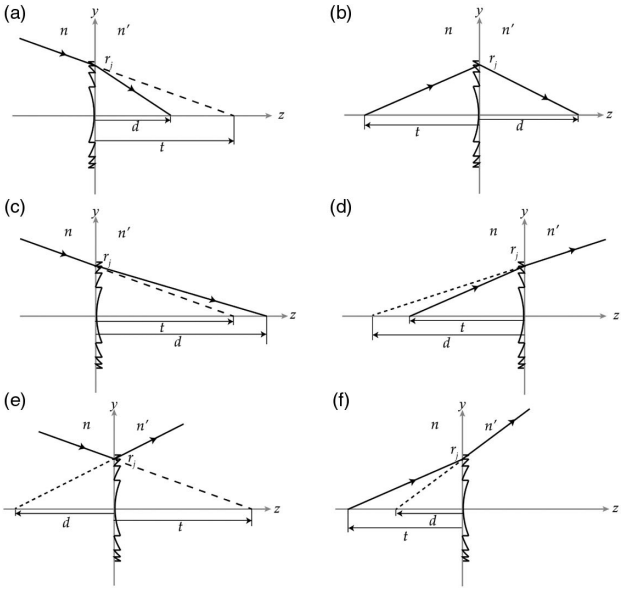

Fig. 13. Fresnel zone boundary determination of a diffractive surface on a flat substrate with converging and diverging beam incidence. (a) Positive power ($\Phi > 0$), converging beam incidence ($t > 0$), and $d > 0$; (b) positive power ($\Phi > 0$), diverging beam incidence ($t < 0$), and $d > 0$; (c) negative power ($\Phi < 0$), converging beam incidence ($t > 0$), and $d > 0$; (d) positive power ($\Phi > 0$), diverging beam incidence ($t < 0$), and $d < 0$; (e) negative power ($\Phi < 0$), converging beam incidence ($t > 0$), and $d < 0$; (f) negative power ($\Phi < 0$), diverging beam incidence ($t < 0$), and $d < 0$.

Here I assume that the diffractive surface semi-aperture r_j of the jth Fresnel zone is significantly smaller than both the incident beam radius and the first focal length of the diffractive surface, yet significantly larger than the design wavelengths, i.e., $d \gg r_j \gg \lambda_0$, and $t \gg r_j \gg \lambda_0$. This assumption is valid for most applications of diffractive optics, including the common use in ophthalmology. Therefore, the terms containing λ_0^2 and r_j^4 can be dropped, and

$$r_j^2 = (2n^2 n' t^2 dj\lambda_0 - 2nn'^2 td^2 j\lambda_0)/(n^2 n'^2 t^2 + n^2 n'^2 d^2 - n^3 n' td - nn'^3 td - n^3 tj\lambda_0 - nn'^2 tj\lambda_0 + n^2 n' dj\lambda_0 + n'^3 dj\lambda_0). \quad (48)$$

The terms containing the factor λ_0 in the denominator are significantly smaller than the other terms in the denominator, and hence can be dropped. Equation (48) is further simplified to

$$r_j^2 = \frac{2j\lambda_0 dt}{-nd + n't} = 2j\lambda_0 d', \quad (49)$$

where

$$d' = d\zeta, \zeta = \frac{t}{-nd + n't}. \quad (50)$$

I shall call ζ the Fresnel zone spacing factor, since it directly scales the spacing of Fresnel zones with respect to $\rho = r^2$. Note that the Fresnel zone spacing factor does not apply only to SMUD lens designs, but also to conventional multifocal diffractive lens designs with full Fresnel zone profiles.

Table 4. Fresnel Zone Boundary Determination of a Diffractive Surface on a Flat Substrate with Converging or Diverging Beam Incidence

$\Phi > 0, t > 0, d > 0$	$-nt + n'd + j\lambda_0 = n'\sqrt{d^2 + r_j^2} - n\sqrt{t^2 + r_j^2}$
	$\zeta = \frac{t}{-nd + n't}$
$\Phi > 0, t < 0, d > 0$	$-nt + n'd + j\lambda_0 = n'\sqrt{d^2 + r_j^2} + n\sqrt{t^2 + r_j^2}$
	$\zeta = \frac{t}{-nd + n't}$
$\Phi > 0, t < 0, d < 0$	$-nt + n'd + j\lambda_0 = -n'\sqrt{d^2 + r_j^2} + n\sqrt{t^2 + r_j^2}$
	$\zeta = \frac{t}{-nd + n't}$
$\Phi < 0, t > 0, d > 0$	$nt - n'd + j\lambda_0 = -n'\sqrt{d^2 + r_j^2} + n\sqrt{t^2 + r_j^2}$
	$\zeta = \frac{t}{nd - n't}$
$\Phi < 0, t > 0, d < 0$	$nt - n'd + j\lambda_0 = n'\sqrt{d^2 + r_j^2} + n\sqrt{t^2 + r_j^2}$
	$\zeta = \frac{t}{nd - n't}$
$\Phi < 0, t < 0, d < 0$	$nt - n'd + j\lambda_0 = n'\sqrt{d^2 + r_j^2} - n\sqrt{t^2 + r_j^2}$
	$\zeta = \frac{t}{nd - n't}$

Equation (49) is linear to the zone number j, and it demonstrates that even with a converging beam incidence, as long as $d \gg r_j \gg \lambda_0$ and $t \gg r_j \gg \lambda_0$, the Fresnel zones are still of equal area, even though this area is scaled, compared with that of plane wave incidence. For a SMUD lens, all the subzone areas are scaled proportionally, compared with those of plane wave incidence.

Correspondingly, with the updated d', the SMUD lens profile can still be summarized as Eq. (43), and if we assume a periodically linear profile in each subzone, the SMUD lens profile is still Eq. (26).

A similar procedure can be analyzed for Figs. 13(b)–13(f), and the results of the corresponding OPL equation at the Fresnel zone boundaries and the Fresnel zone spacing factor ζ are summarized in Table 4.

Table 4 illustrates that although the OPL equations are different for different lens geometries, the Fresnel zone spacing factor is dependent on the sign of the lens power Φ, and can be summarized as

$$\zeta = \mathrm{sgn}(\Phi)\frac{t}{-nd + n't}. \quad (51)$$

Further, when $t \to \infty$, $\zeta \to \mathrm{sgn}(\Phi)/n'$, $d' \to |d|/n'$, where $\mathrm{sgn}(\Phi)$ is the sign function, and the above analysis reduces to our previous analysis for plane wave incidence.

The converging or diverging incident beam will introduce an extra factor in the transmission function. With paraxial approximation, the extra factor has the form of $\exp(-\frac{i2\pi nt}{\lambda})\exp(-\frac{i\pi n}{\lambda t}r^2)/|t|$. The $1/|t|$ factor comes from energy conservation, but it will not affect the energy

distribution among different foci. The $\exp(-\frac{i2\pi nt}{\lambda})$ term is independent of ρ and vanishes in η_m after multiplying with its conjugate. Therefore, only the quadratic phase of $\exp[-\frac{i\pi n(\lambda)}{\lambda t}r^2] = \exp[-\frac{i\pi n(\lambda)}{\lambda t}\rho]$ has to be taken into account.

With converging or diverging incidence for a SMUD lens on a flat substrate, which is periodically linear in ρ as described in Eqs. (26) and (36), the Fourier coefficient is

$$
\begin{aligned}
c_m = {} & \gamma_1 e^{i\pi\gamma_1\left(m-\alpha\beta_1-\frac{n\lambda_0 d'}{\lambda t}\right)}\operatorname{sinc}\left[\gamma_1\left(m-\alpha\beta_1-\frac{n\lambda_0 d'}{\lambda t}\right)\right] \\
& + (\gamma_2-\gamma_1)e^{i\pi(\gamma_2+\gamma_1)\left(m-\alpha\beta_2-\frac{n\lambda_0 d'}{\lambda t}\right)} \\
& \times \operatorname{sinc}\left[(\gamma_2-\gamma_1)\left(m-\alpha\beta_2-\frac{n\lambda_0 d'}{\lambda t}\right)\right] \\
& + \ldots \\
& + (\gamma_g-\gamma_{g-1})e^{i\pi(\gamma_g+\gamma_{g-1})\left(m-\alpha\beta_g-\frac{n\lambda_0 d'}{\lambda t}\right)} \\
& \times \operatorname{sinc}\left[(\gamma_g-\gamma_{g-1})\left(m-\alpha\beta_g-\frac{n\lambda_0 d'}{\lambda t}\right)\right] \\
& + \ldots \\
& + (1-\gamma_{G-1})e^{i\pi(1+\gamma_{G-1})\left(m-\alpha\beta_G-\frac{n\lambda_0 d'}{\lambda t}\right)} \\
& \times \operatorname{sinc}\left[(1-\gamma_{G-1})\left(m-\alpha\beta_G-\frac{n\lambda_0 d'}{\lambda t}\right)\right]. \qquad (52)
\end{aligned}
$$

All the formulas of the Fourier coefficients c_m and η_m can be updated accordingly for SMUD lenses.

7. CURVED SUBSTRATE

The substrate surface for a multifocal diffractive lens is not necessarily a flat surface. When the diffractive lens is formed on a curved substrate surface, a Fresnel zone spacing factor has to be taken into account, and an extra phase in the transmission function will adjust the energy allocation among different foci.

I shall start with the cases of plane wave incidence for a diffractive surface on a curved substrate. R is the radius of the substrate, $R<0$ corresponds to a convex substrate, since the lens material is to the left, and $R>0$ corresponds to a concave surface.

Figure 14 presents four different cases of a converging incidence beam with a positive or negative diffractive surface on a convexly or concavely curved substrate.

The OPL equation at the Fresnel zone boundaries in Fig. 14(a) is

$$-ns_j + n'd + j\lambda_0 = n'\sqrt{(d-s_j)^2+r_j^2}, \qquad (53)$$

where s_j is the sag of the jth zone, and

$$s_j = \begin{cases} R-\sqrt{R^2-r_j^2}, & R>0 \\ R+\sqrt{R^2-r_j^2}, & R<0 \end{cases}. \qquad (54)$$

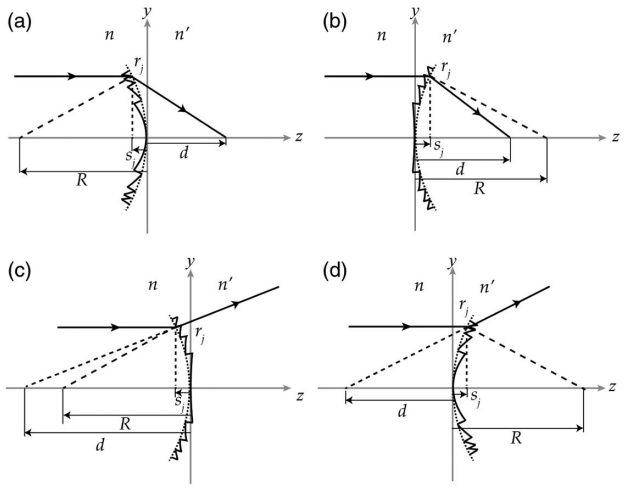

Fig. 14. Fresnel zone boundary determination of a diffractive surface on a curved substrate with plane wave incidence. (a) Positive power ($d>0$) with a convex lens substrate ($R<0$); (b) positive power ($d>0$) with a concave lens substrate ($R>0$); (c) negative power ($d<0$) with convex lens substrate ($R<0$); (d) negative power ($d<0$) with a concave lens substrate ($R>0$).

For most applications, $R \gg r_j \gg \lambda_0$. Keeping only the first two lower-order terms of the Taylor series expansion of the square root in Eq. (54), the sag can be approximated further as

$$s_j = \frac{r_j^2}{2R}. \qquad (55)$$

Square both sides of Eq. (53), drop the small higher-order terms containing r_j^4 and λ_0^2, and use the approximation of Eq. (55) to obtain

$$r_j^2 = \frac{2j\lambda_0 dn'}{n'^2 - n'^2\frac{d}{R} + nn'\frac{d}{R} + nj\frac{\lambda_0}{R}}. \qquad (56)$$

Since $d \gg \lambda_0$, the term containing λ_0 in the denominator is small and can be dropped; hence,

$$
\begin{aligned}
r_j^2 &= \frac{2j\lambda_0 dn'}{n'^2 - n'^2\frac{d}{R} + nn'\frac{d}{R}} \\
&= \frac{2j\lambda_0 d}{n' + (n-n')\frac{d}{R}} = 2j\lambda_0 d', \qquad (57)
\end{aligned}
$$

where

$$d' = d\zeta,\ \zeta = \frac{1}{n' + (n-n')\frac{d}{R}}. \qquad (58)$$

A similar procedure can be performed for Figs. 14(b)–14(d), and the results of the corresponding OPL equation at the Fresnel zone boundaries and the Fresnel zone spacing factor ζ are summarized in Table 5.

Table 5 demonstrates that the Fresnel zone spacing factor is dependent on the sign of the lens power Φ, and can be summarized as

$$\zeta = \operatorname{sgn}(\Phi)\frac{1}{n' + (n-n')d/R}. \qquad (59)$$

Table 5. Fresnel Zone Boundary Determination of a Diffractive Surface on a Curved Substrate with Plane Wave Incidence[a]

$\Phi > 0\,(d > 0)$	$-ns_j + n'd + j\lambda_0 = n'\sqrt{(d - s_j)^2 + r_j^2}$
	$\zeta = \frac{1}{n' + (n - n')d/R}$
$\Phi < 0\,(d < 0)$	$ns_j - n'd + j\lambda_0 = n'\sqrt{(s_j - d)^2 + r_j^2}$
	$\zeta = \frac{1}{-n' - (n - n')d/R}$

[a]The mathematical forms of the OPL equations at the zone boundaries and the Fresnel zone spacing factors ζ are independent of the sign of R.

When $R \to \infty$, the substrate becomes flat, which has been analyzed before, $\zeta \to \mathrm{sgn}(\Phi)/n'$, and $d' = |d|/n'$.

With paraxial approximation, the surface sag s_j will cause an extra quadratic phase of $\exp\{ik(\lambda)[n(\lambda) - n'(\lambda)]\frac{r^2}{2R}\} = \exp\{\frac{i\pi[n(\lambda)-n'(\lambda)]\rho}{\lambda R}\}$, which has to be taken into account.

With plane wave incidence for a SMUD lens on a curved substrate, which is periodically linear in ρ as described in Eqs. (26) and (36), the Fourier coefficient

$$
\begin{aligned}
c_m = {} & \gamma_1 \mathrm{e}^{i\pi\gamma_1\left[m - \alpha\beta_1 + \frac{(n-n')\lambda_0 d'}{\lambda R}\right]} \\
& \times \mathrm{sinc}\left\{\gamma_1\left[m - \alpha\beta_1 + \frac{(n-n')\lambda_0 d'}{\lambda R}\right]\right\} \\
& + (\gamma_2 - \gamma_1)\mathrm{e}^{i\pi(\gamma_2+\gamma_1)\left[m - \alpha\beta_2 + \frac{(n-n')\lambda_0 d'}{\lambda R}\right]} \\
& \times \mathrm{sinc}\left\{(\gamma_2 - \gamma_1)\left[m - \alpha\beta_2 + \frac{(n-n')\lambda_0 d'}{\lambda R}\right]\right\} \\
& + \ldots \\
& + (\gamma_g - \gamma_{g-1})\mathrm{e}^{i\pi(\gamma_g+\gamma_{g-1})\left[m - \alpha\beta_g + \frac{(n-n')\lambda_0 d'}{\lambda R}\right]} \\
& \times \mathrm{sinc}\left\{(\gamma_g - \gamma_{g-1})\left[m - \alpha\beta_g + \frac{(n-n')\lambda_0 d'}{\lambda R}\right]\right\} \\
& + \ldots \\
& + (1 - \gamma_{G-1})\mathrm{e}^{i\pi(1+\gamma_{G-1})\left[m - \alpha\beta_G + \frac{(n-n')\lambda_0 d'}{\lambda R}\right]} \\
& \times \mathrm{sinc}\left\{(1 - \gamma_{G-1})\left[m - \alpha\beta_G + \frac{(n-n')\lambda_0 d'}{\lambda R}\right]\right\}. \qquad (60)
\end{aligned}
$$

All the formulas of the Fourier coefficients c_m and η_m can be updated accordingly.

Next, I shall analyze the cases with converging beam incidence on a curved substrate. Figure 15 presents six different cases of a converging incident beam with a positive or negative diffractive surface on a convexly or concavely curved substrate.

Referring to Fig. 15(a), a converging beam ($t > 0$) is incident on a positive diffractive surface ($\Phi > 0$) on a convex substrate ($R < 0$). The OPL equation at the Fresnel boundaries is

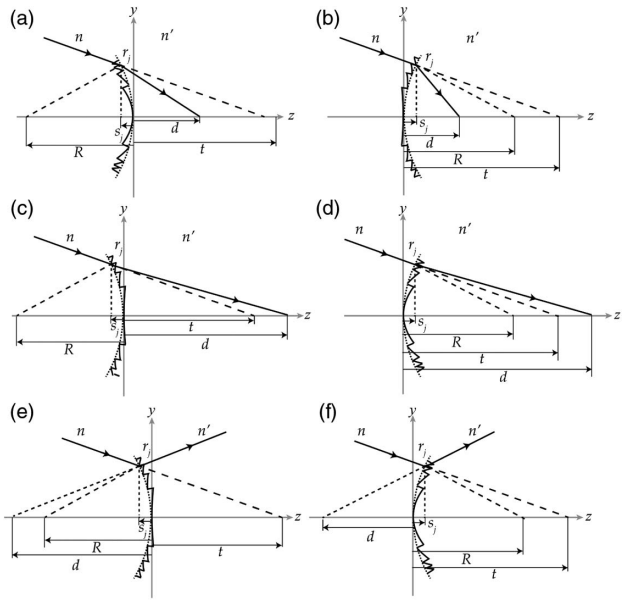

Fig. 15. Fresnel zone boundary determination of a diffractive surface on a curved substrate with converging beam incidence ($t > 0$). (a) $t > 0$, $\Phi > 0$, $d > 0$, $R < 0$; (b) $t > 0$, $\Phi > 0$, $d > 0$, $R > 0$; (c) $t > 0$, $\Phi < 0$, $d > 0$, $R < 0$; (d) $t > 0$, $\Phi < 0$, $d > 0$, $R > 0$; (e) $t > 0$, $\Phi < 0$, $d < 0$, $R < 0$; (f) $t > 0$, $\Phi < 0$, $d < 0$, $R > 0$.

$$
-nt + n'd + j\lambda_0 = n'\sqrt{(d - s_j)^2 + r_j^2} - n\sqrt{(t - s_j)^2 + r_j^2}. \qquad (61)
$$

Equation (61) can be rearranged as

$$
\begin{aligned}
& (2nn'td + 2ntj\lambda_0 - 2n'dj\lambda_0 - 2n^2ts_j - 2n'^2ds_j + n^2r_j^2 \\
& \quad + n'^2r_j^2 + n^2s_j^2 + n'^2s_j^2 - j^2\lambda_0^2)^2 = 4n^2n'^2 \\
& \quad \times [(t^2 - 2ts_j + s_j^2 + r_j^2)(d^2 - 2ds_j + s_j^2 + r_j^2)]. \qquad (62)
\end{aligned}
$$

With the assumption $d \gg r_j \gg \lambda_0$, $t \gg r_j \gg \lambda_0$, and $R \gg r_j \gg \lambda_0$, the higher-order terms containing λ_0^2, r_j^4, s_j^2, and $s_j r_j^2$ can be dropped, and

$$
\begin{aligned}
r_j^2 = {} & (2n^2n't^2dj\lambda_0 - 2nn'^2td^2j\lambda_0)/(-n^2n'^2td^2/R \\
& + n^2n'^2d^2 - n^2n'^2t^2d/R + n^2n'^2t^2 + nn'^3td^2/R \\
& - n^3n'td - nn'^3td + n^3n't^2d/R + nn'^2tdj\lambda_0/R \\
& - n'^3d^2j\lambda_0/R - n^3tj\lambda_0 + n'^3dj\lambda_0 + n^3t^2j\lambda_0/R \\
& - n^2n'tdj\lambda_0/R + n'n^2dj\lambda_0 - nn'^2tj\lambda_0). \qquad (63)
\end{aligned}
$$

The terms containing λ_0 in the denominator are small compared with other terms in the denominator, and can be further dropped, so Eq. (63) can be simplified as

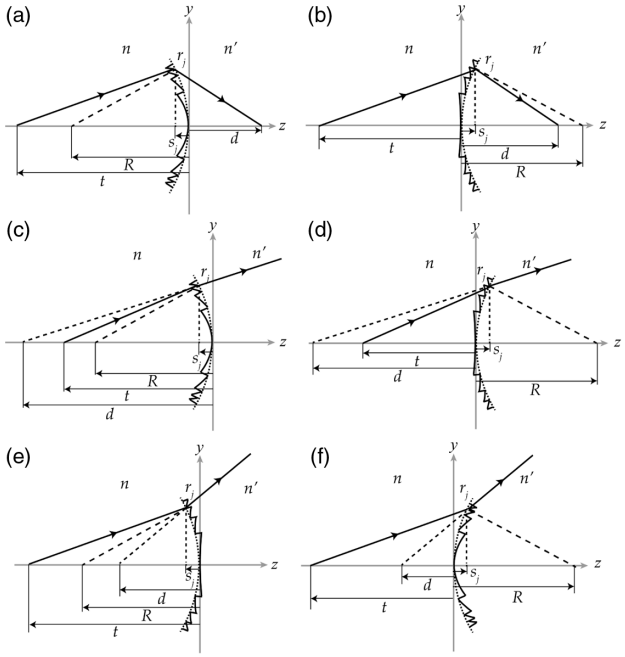

Fig. 16. Fresnel zone boundary determination of a diffractive surface on a curved substrate with diverging beam incidence ($t<0$). (a) $t<0, \Phi>0, d>0, R<0$; (b) $t<0, \Phi>0, d>0, R>0$; (c) $t<0, \Phi>0, d<0, R<0$; (d) $t<0, \Phi>0, d<0, R>0$; (e) $t<0, \Phi<0, d<0, R<0$; (f) $t<0, \Phi<0, d<0, R>0$.

$$r_j^2=[2nn'tdj\lambda_0(nt-n'd)]/[nn'^2t(nt-n'd)$$
$$-n^2n'd(nt-n'd)-\frac{nn'^2td}{R}(nt-n'd)$$
$$+\frac{n^2n'td}{R}(nt-n'd)]$$
$$=2j\lambda_0 d\frac{t}{n't-nd+\frac{td}{R}(n-n')}$$
$$=2j\lambda_0 d', \tag{64}$$

where

$$d'=d\zeta,\quad \zeta=\frac{t}{n't-nd+\frac{td}{R}(n-n')}. \tag{65}$$

A similar procedure can be performed for Figs. 15(b)–15(f) of converging beam incidence and Figs. 16(a)–16(f) of diverging beam incidence, and the results of the corresponding OPL equation at the Fresnel zone boundaries and the Fresnel zone spacing factor ζ are summarized in Table 6. Note that for $d>0$, even though the original OPL equations at the zone boundaries are different for $t>0$ and $t<0$, after simplification, the Fresnel zone spacing factors ζ for both $t>0$ and $t<0$ are the same. The same conclusion also applies for the case of $d<0$.

Further, when $t\to\infty$, the incident beam becomes plane wave, and Table 6 reduces to Table 5.

When $R\to\infty$, the substrate becomes flat, and Table 6 reduces to Table 4.

Table 6. Fresnel Zone Boundary Determination of a Diffractive Surface on a Curved Substrate with Converging ($t>0$) or Diverging ($t<0$) Beam Incidence[a]

$\Phi>0, t>0, d>0$	$-nt+n'd+j\lambda_0=n'\sqrt{(d-s_j)^2+r_j^2}-n\sqrt{(t-s_j)^2+r_j^2}$
	$\zeta=\frac{t}{n't-nd+(n-n')td/R}$
$\Phi>0, t<0, d>0$	$-nt+n'd+j\lambda_0=n'\sqrt{(d-s_j)^2+r_j^2}+n\sqrt{(t-s_j)^2+r_j^2}$
	$\zeta=\frac{t}{n't-nd+(n-n')td/R}$
$\Phi>0, t<0, d<0$	$-nt+n'd+j\lambda_0=-n'\sqrt{(d-s_j)^2+r_j^2}+n\sqrt{(t-s_j)^2+r_j^2}$
	$\zeta=\frac{t}{n't-nd+(n-n')td/R}$
$\Phi<0, t>0, d>0$	$nt-n'd+j\lambda_0=-n'\sqrt{(d-s_j)^2+r_j^2}+n\sqrt{(t-s_j)^2+r_j^2}$
	$\zeta=\frac{t}{-n't+nd-(n-n')td/R}$
$\Phi<0, t>0, d<0$	$nt-n'd+j\lambda_0=n'\sqrt{(d-s_j)^2+r_j^2}+n\sqrt{(t-s_j)^2+r_j^2}$
	$\zeta=\frac{t}{-n't+nd-(n-n')td/R}$
$\Phi<0, t<0, d<0$	$nt-n'd+j\lambda_0=n'\sqrt{(d-s_j)^2+r_j^2}-n\sqrt{(t-s_j)^2+r_j^2}$
	$\zeta=\frac{t}{-n't+nd-(n-n')td/R}$

[a]The mathematical forms of the OPL equations at the zone boundaries and the Fresnel zone spacing factors ζ are independent of the sign of R.

When $t\to\infty$, and $R\to\infty$, $d'\to|d|/n'$, and the above analysis reduces to the previous analysis for a flat substrate with plane wave incidence.

Similar to Eq. (49), the Fresnel zone boundaries of the configurations drawn in Figs. 14–16 are all linear to the zone number j, and it demonstrates that for a diffractive surface on a curved substrate with planar or spherical wave incidence, as long as $d\gg r_j\gg\lambda_0$, $t\gg r_j\gg\lambda_0$ and $R\gg r_j\gg\lambda_0$, the optimal Fresnel zones are still of equal area, even though this area is scaled by a Fresnel zone spacing factor ζ, compared with that of a diffractive surface on a flat substrate in ambient air with plane wave incidence. For a SMUD lens, all the subzone areas are scaled proportionally.

Table 6 demonstrates that the Fresnel zone spacing factor is dependent on the sign of the lens power Φ, and can be summarized as

$$\zeta=\mathrm{sgn}(\Phi)\frac{t}{n't-nd+(n-n')td/R}. \tag{66}$$

With converging or diverging beam incidence for a SMUD lens on a curved substrate, which is periodically linear in ρ as described in Eqs. (26) and (36), the Fourier coefficient is

$$
\begin{aligned}
c_m = {} & \gamma_1 e^{i\pi\gamma_1\left[m-\alpha\beta_1-\frac{n\lambda_0 d'}{\lambda t}+\frac{(n-n')\lambda_0 d'}{\lambda R}\right]} \\
& \times \operatorname{sinc}\left\{\gamma_1\left[m-\alpha\beta_1-\frac{n\lambda_0 d'}{\lambda t}+\frac{(n-n')\lambda_0 d'}{\lambda R}\right]\right\} \\
& + (\gamma_2-\gamma_1) e^{i\pi(\gamma_2+\gamma_1)\left[m-\alpha\beta_2-\frac{n\lambda_0 d'}{\lambda t}+\frac{(n-n')\lambda_0 d'}{\lambda R}\right]} \\
& \times \operatorname{sinc}\left\{(\gamma_2-\gamma_1)\left[m-\alpha\beta_2-\frac{n\lambda_0 d'}{\lambda t}+\frac{(n-n')\lambda_0 d'}{\lambda R}\right]\right\} \\
& + \ldots \\
& + (\gamma_g-\gamma_{g-1}) e^{i\pi(\gamma_g+\gamma_{g-1})\left[m-\alpha\beta_g-\frac{n\lambda_0 d'}{\lambda t}+\frac{(n-n')\lambda_0 d'}{\lambda R}\right]} \\
& \times \operatorname{sinc}\left\{(\gamma_g-\gamma_{g-1})\left[m-\alpha\beta_g-\frac{n\lambda_0 d'}{\lambda t}+\frac{(n-n')\lambda_0 d'}{\lambda R}\right]\right\} \\
& + \ldots \\
& + (1-\gamma_{G-1}) e^{i\pi(1+\gamma_{G-1})\left[m-\alpha\beta_G-\frac{n\lambda_0 d'}{\lambda t}+\frac{(n-n')\lambda_0 d'}{\lambda R}\right]} \\
& \times \operatorname{sinc}\left\{(1-\gamma_{G-1})\left[m-\alpha\beta_G-\frac{n\lambda_0 d'}{\lambda t}+\frac{(n-n')\lambda_0 d'}{\lambda R}\right]\right\}. \qquad (67)
\end{aligned}
$$

All the formulas of the Fourier coefficients c_m and η_m can be updated accordingly for SMUD lenses. Therefore, a curved substrate and/or a converging or diverging beam incidence will demand changes in the boundaries of the Fresnel zone and the corresponding subzones. The diffraction efficiency analysis also has to be adjusted by taking into account the incidence beam shape and the substrate curvature.

8. APODIZATION

In order to emphasize distant vision over near vision in mesopic conditions, and to reduce glares and halos in dim conditions such as nighttime driving, apodization in diffraction efficiency was introduced [11]. Conventional apodization in optical systems usually means a gradually decreasing transparency towards the periphery of a pupil [17]. In multifocal diffractive lenses, apodization means decreasing diffraction efficiency into higher orders by gradually lowering the step heights towards the diffractive lens periphery.

In the mathematical framework of this paper, apodization essentially means continuously decreasing the phase step factor β or all β_s for SMUD lenses with r or ρ. The original apodization factor proposed by Lee and Simpson [24] can be absorbed into β as

$$
\begin{aligned}
\beta &= \beta_0 f_{\text{apodize}} = \beta_0\left[1-\left(\frac{r-r_{\text{in}}}{r_{\text{out}}-r_{\text{in}}}\right)^e\right], \\
& r_{\text{in}} \le r \le r_{\text{out}} \qquad (68)
\end{aligned}
$$

where f_{apodize} is the apodization factor, and r_{in} and r_{out} are the inner and outer boundaries of the apodized region. e is an exponent. β_0 is the phase step factor if there is no apodization.

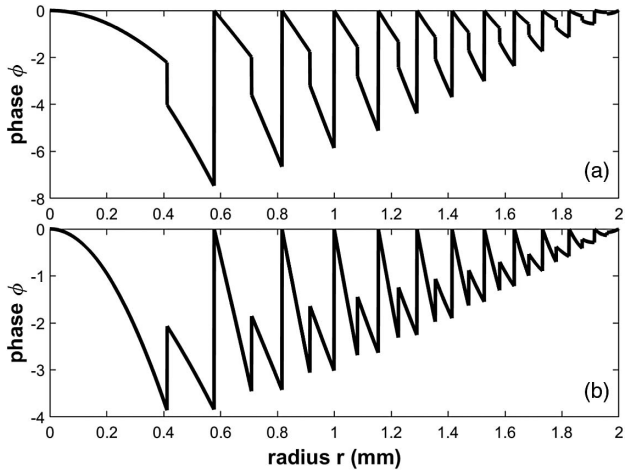

Fig. 17. Phase profile with the apodization factor in the form of Eq. (70) for (a) design #3 and (b) #4. $r_{\text{in}} = 0$ mm, $r_{\text{out}} = 2$ mm, $e_1 = 1$.

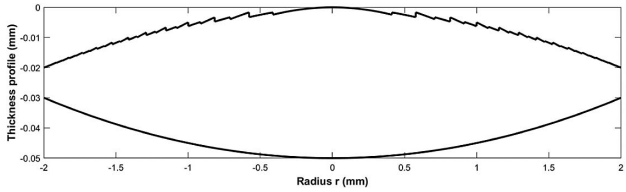

Fig. 18. Combination of an apodized diffractive surface in Fig. 17(b) and a refractive base lens.

The basic concept of apodization can be understood by referring to Fig. 3. If we focus in the range of $\beta \in [0, 1]$, as β approaches zero, the zeroth-order diffraction efficiency approaches one, while that of all other orders approaches zero.

Note that any function that monotonically decreases with radius r could potentially be used as an apodization factor, and all these apodization factors could be applied to SMUD lenses. For example, here I propose a novel type of the apodization factor:

$$
f_{\text{apodize1}} = \cos^{e_2}\left[\frac{\pi}{2}\left(\frac{r-r_{\text{in}}}{r_{\text{out}}-r_{\text{in}}}\right)^{e_1}\right], \qquad (69)
$$

where $e_1, e_2 > 0$ are two positive exponents. When $e_2 = 1$, Eq. (69) reduces to

$$
f_{\text{apodize2}} = \cos\left[\frac{\pi}{2}\left(\frac{r-r_{\text{in}}}{r_{\text{out}}-r_{\text{in}}}\right)^{e_1}\right]. \qquad (70)
$$

If $e_2 > 1$, f_{apodize1} always decreases faster than f_{apodize2}, and if $0 < e_2 < 1$, f_{apodize1} always decreases slower than f_{apodize2}. The larger e_1 is, the slower the apodization factor drops near the center, and the more steeply it declines when r reaches the edge of the apodized region.

Two exemplary apodization profiles are shown in Fig. 17. Further, Fig. 18 presents a thickness profile of a diffractive surface combined with a refractive base lens. The diffractive surface is from design #4 with an apodization factor of Fig. 17(b).

A varying β across different Fresnel zones violates the periodicity in ρ; hence, the diffraction efficiencies of different orders could no longer be directly calculated from Fourier coefficients in the Fourier series expansion of the transmission function of a single Fresnel zone period. However, Eqs. (9) and (10) can still be used to estimate the local diffraction efficiency based on the local spatial frequency, as if the local periodicity of the region under investigation extends to a large scale [25].

9. OPHTHALMIC ASTIGMATISM

Astigmatism in optical engineering is one of the five Seidel aberrations, and for a rotationally symmetric system, astigmatism exists only for off-axis field points [26]. In contrast, ophthalmic astigmatism refers to the difference in optical powers in different meridians, which means that the rotational symmetry is broken, and it corresponds to a cylinder power in a certain meridian plane in optical engineering. Therefore, ophthalmic astigmatism is present even for the on-axis field points.

In all the previous analyses, a circularly symmetric system was assumed. However, in order to correct vision for patients with ophthalmic astigmatism, different powers along two orthogonal meridian planes should be generated and aligned with the patient's astigmatic axes.

The cylinder power can be added to a diffractive surface with different spacing in two orthogonal planes [12]. If a Cartesian coordinate system is chosen such that the astigmatic cylinder power axis is along the x or y axis, the zone boundaries along the x and y axes are

$$r_{xj}^2 = 2j\lambda_0 d_x', \tag{71}$$

$$r_{yj}^2 = 2j\lambda_0 d_y'. \tag{72}$$

The jth zone boundary follows [12]:

$$\frac{x^2}{2j\lambda_0 d_x'} + \frac{y^2}{2j\lambda_0 d_y'} = 1. \tag{73}$$

The zone boundaries of a diffractive lens with rotational symmetry and one with cylinder power are shown in Fig. 19.

Similarly, hyperbolic zone boundaries could also be used to generate a cylinder power [12].

For a multifocal diffractive lens, if a basic spherical power of $1/d_x'$ is chosen, for mth order, the cylinder power is

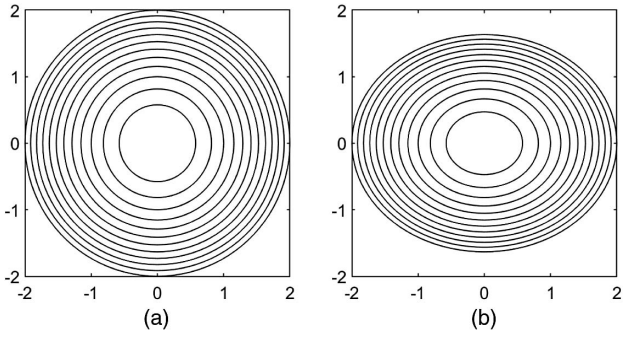

Fig. 19. Zone boundaries of (a) rotationally symmetric diffractive lens ($d' = 300$ mm) and (b) one diffractive lens with a cylinder power ($d_x' = 300$ mm, $d_y' = 200$ mm).

$$\Phi_{\text{cylinder}} = \frac{1}{f_{my}} - \frac{1}{f_{mx}} = m\left(\frac{1}{d_y'} - \frac{1}{d_x'}\right). \tag{74}$$

Hence, the cylinder power will vary for different diffraction orders, and it is proportional to the order m. For diffractive lenses used in ophthalmology, the added astigmatism is usually used to correct a fixed residual astigmatism in other parts of the eye; for example, the added astigmatism of an intraocular lens is usually chosen to cancel the corneal astigmatism. Multifocal diffractive lenses with elliptical or hyperbolic outlines can correct residual astigmatism for only one order and will introduce additional astigmatism for all other orders. Hence, to compensate for a fixed ophthalmic astigmatism, a diffractive surface with elliptical or hyperbolic boundaries is applicable for only monofocal diffractive lenses.

Moreover, to introduce a fixed cylinder power, the diffractive lens with elliptical boundaries in Fig. 19(b) requires plane wave incidence and a flat substrate. As presented in Eq. (67), the Fourier coefficient c_m and the corresponding diffraction efficiency η_m are dependent on the spacing d', with converging/diverging beam incidence or a curved substrate. Hence, if the diffractive lens is monofocal in the x-meridian plane, it is likely not monofocal in the y-meridian plane. The cylinder power at all other orders will serve as the background noise to lower the image contrast, even for a nominally "monofocal" lens.

This difficulty of introducing a fixed cylinder power for different diffraction orders applies to all multifocal diffractive lenses, including SMUD lenses. Therefore, the diffractive lenses with elliptical or hyperbolic outlines are rarely used in ophthalmology.

Instead, toric intraocular lenses are usually used to correct for ophthalmic astigmatism [13–15]. The cylinder power is provided via different optical powers in two orthogonal meridian planes by a refractive toric lens. A toric surface can be combined with a multifocal diffractive surface to generate different multiorder optical powers with a fixed astigmatism-correction cylinder power. The toric surface and the diffractive surface could be on the opposite side of a lens, or the toric lens and the multifocal diffractive lens could be separate optics.

10. DISCUSSION

In this paper, a generalized mathematical description is developed to summarize multifocal diffractive lens designs. Novel SMUD lens designs are introduced with analytical and numerical methods. Some further considerations are discussed below.

(1) The phase profile can be approximated by a series of steps with a constant phase in each subzone, and in the case where the profile is approximated by 2^n steps of equal step height, a SMUD lens reduces to a binary lens.

(2) Most examples analyzed in this paper have a sawtooth-like thickness profile to create a phase step at the zone boundaries. The sawtooth profile can be avoided by combining two materials of different refractive indices with matching profiles, so that the sawtooth pattern is embedded in the interior of the combined lens, while the exterior of the lens

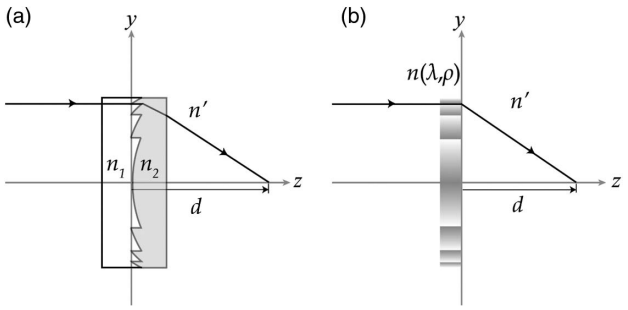

Fig. 20. (a) Diffractive lens combining two materials of different refractive indices with matching profiles; (b) diffractive lens with gradient refractive index periodic in ρ.

can be smooth [8]. This is shown in Fig. 20(a). The two materials can be optically connected together with index matching adhesives. Alternatively, the two materials could be formed from one base material, and part of the material has the refractive index changed to a different value by methods such as doping or laser writing. The transmission function

$$t(\rho) = A(\rho)\exp\{ik(\lambda)[n_1(\lambda) - n_2(\lambda)]\delta(\rho)\}. \quad \textbf{(75)}$$

(3) Further, the phase step without a sawtooth-like thickness profile can also be created by periodically altering the refractive index of portions of the material by means of ion exchange, partial polymerization, laser writing, doping, etc. [27], as shown in Fig. 20(b). Hence, instead of a thickness profile, a refractive index profile could be used to generate the desired phase profile. The transmission function

$$t(\rho) = A(\rho)\exp[ik(\lambda)n(\lambda,\rho)\delta_c], \quad \textbf{(76)}$$

where δ_c is a constant thickness, and $n(\lambda,\rho)$ is a gradient refractive index periodic in ρ. Analogous to Eq. (16), for a periodically linear gradient refractive index profile,

$$\phi(\rho;\lambda) = k(\lambda)n_0(\lambda)\left(j - \frac{\rho}{2\lambda_0 d'}\right)\delta_c$$

$$= 2\pi\alpha_{\mathrm{GI}}\beta_{\mathrm{GI}}\left(j - \frac{\rho}{2\lambda_0 d'}\right), \quad \textbf{(77)}$$

where the subscript "GI" stands for "gradient index," and the gradient index profile is

$$n(\lambda,\rho) = n_0(\lambda)[j - \rho/(2\lambda_0 d')]. \quad \textbf{(78)}$$

α_{GI} and β_{GI} are

$$\alpha_{\mathrm{GI}} = \frac{\phi(\lambda)}{\phi(\lambda_0)} = \frac{\lambda_0 n_0(\lambda)}{\lambda n_0(\lambda_0)}, \quad \textbf{(79)}$$

$$\beta_{\mathrm{GI}} = n_0(\lambda_0)\delta_c/\lambda_0. \quad \textbf{(80)}$$

Substituting "α_{GI}" for "α" and "β_{GI}" for "β", previously derived Eqs. (26), (27), (36), (42), and (43) could all be applied directly to a SMUD gradient index lens.

Obviously, it is also possible to vary both the thickness and the refractive index with ρ to achieve a desired phase profile.

Disclosures. The author is the inventor of a related patent application [22]. AZ: (P).

REFERENCES

1. M. Brass, J. Enoch, E. Van Stryland, and W. Wolfe, *Handbook of Optics (Volume III): Vision and Vision Optics* (McGraw-Hill Education, 2010).
2. N. Congdon, J. Vingerling, B. Klein, S. West, D. Friedman, J. Kempen, B. O'Colmain, S. Wu, and H. Taylor, "Prevalence of cataract and pseudophakia/aphakia among adults in the United States," Arch. Ophthalmol. **122**, 487–494 (2004).
3. W. Wang, W. Yan, K. Fotis, N. M. Prasad, V. C. Lansingh, H. R. Taylor, R. P. Finger, D. Facciolo, and M. He, "Cataract surgical rate and socioeconomics: a global study," Invest. Ophthalmol. Visual Sci. **57**, 5872–5881 (2016).
4. H. Hashemi, R. Pakzad, A. Yekta, M. Aghamirsalim, M. Pakbin, S. Ramin, and M. Khabazkhoob, "Global and regional prevalence of age-related cataract: a comprehensive systematic review and meta-analysis," Eye **34**, 1357–1370 (2020).
5. M. Leyland and E. Zinicola, "Multifocal versus monofocal intraocular lenses in cataract surgery: a systematic review," Ophthalmology **110**, 1789–1798 (2003).
6. J. Woods, C. Woods, and D. Fonn, "Visual performance of a multifocal contact lens versus monovision in established presbyopes," Optometry Vis. Sci. **92**, 175–182 (2015).
7. R. Bellucci, "Multifocal intraocular lenses," Curr. Opin. Ophthalmol. **16**, 33–37 (2005).
8. A. L. Cohen, "Multifocal zone plate," U.S. patent 4,210,391 (1 July 1980).
9. A. L. Cohen, "Phase shift multifocal zone plate," U.S. patent 4,340,283 (20 July 1982).
10. J. A. Futhey, "Diffractive lens," U.S. patent 4,936,666 (26 June 1990).
11. J. A. Davison and M. J. Simpson, "History and development of the apodized diffractive intraocular lens," J. Cataract Refract. Surg. **32**, 849–858 (2006).
12. D. Baude, P. Chavel, D. Joyeux, and J. Taboury, "Optical lens for correcting astigmatism," U.S. patent 5,016,977 (21 May 1991).
13. C. Novis, "Astigmatism and toric intraocular lenses," Curr. Opin. Ophthalmol. **11**, 47–50 (2000).
14. X.-Y. Sun, D. Vicary, P. Montgomery, and M. Griffiths, "Toric intraocular lenses for correcting astigmatism in 130 eyes," Ophthalmology **107**, 1776–1781 (2000).
15. N. J. Bauer, N. E. de Vries, C. A. Webers, F. Hendrikse, and R. M. Nuijts, "Astigmatism management in cataract surgery with the Acrysof toric intraocular lens," J. Cataract Refract. Surg. **34**, 1483–1488 (2008).
16. D. A. Buralli, G. M. Morris, and J. R. Rogers, "Optical performance of holographic kinoforms," Appl. Opt. **28**, 976–983 (1989).
17. J. W. Goodman, *Introduction to Fourier Optics* (McGraw-Hill, 2008).
18. H. Dammann, "Blazed synthetic phase-only holograms," Optik **31**, 95–104 (1970).
19. J. A. Futhey, "Diffractive bifocal intraocular lens," Proc. SPIE **1052**, 142–150 (1989).
20. D. Faklis and G. M. Morris, "Spectral properties of multiorder diffractive lenses," Appl. Opt. **34**, 2462–2468 (1995).
21. D. C. O'Shea, T. J. Suleski, A. D. Kathman, and D. W. Prather, *Diffractive Optics: Design, Fabrication, and Test* (SPIE, 2004), Vol. **62**.
22. A. Zhang, "Subzonal multifocal diffractive lens," U.S. patent application 16/368826 (28 March 2019).
23. J. T. Schwiegerling, "Diffractive trifocal lens," U.S. patent 9,320,594 (26 April 2016).
24. C.-S. Lee and M. J. Simpson, "Diffractive multifocal ophthalmic lens," U.S. patent 5,699,142 (16 December 1997).
25. W. Welford, "A vector raytracing equation for hologram lenses of arbitrary shape," Opt. Commun. **14**, 322–323 (1975).
26. W. J. Smith, *Modern Optical Engineering* (Tata McGraw-Hill Education, 2008).
27. D. T. Moore, "Gradient-index optics: a review," Appl. Opt. **19**, 1035–1038 (1980).